UNIVERSITY *of* York

This is a repository copy of *Measurement of the α ratio and (n,γ) cross section of U 235 from 0.2 to 200 eV at n_TOF MEASUREMENT of the α RATIO and ... J. BALIBREA-CORREA et al.*.

White Rose Research Online URL for this paper:
https://eprints.whiterose.ac.uk/id/eprint/173555/

Version: Published Version

Article:

(2020) Measurement of the α ratio and (n,γ) cross section of U 235 from 0.2 to 200 eV at n_TOF MEASUREMENT of the α RATIO and ... J. BALIBREA-CORREA et al. Physical Review C. 044615. ISSN: 2469-9993

https://doi.org/10.1103/PhysRevC.102.044615

White Rose
university consortium
Universities of Leeds, Sheffield & York

eprints@whiterose.ac.uk
https://eprints.whiterose.ac.uk/

Measurement of the α ratio and (n, γ) cross section of ^{235}U from 0.2 to 200 eV at n_TOF

J. Balibrea-Correa,[1] E. Mendoza [ORCID],[1,*] D. Cano-Ott,[1] E. González,[2] R. Capote,[3] M. Krtička,[4] S. Altstadt,[5] J. Andrzejewski,[6] L. Audouin,[7] V. Bécares,[2] M. Barbagallo,[8] F. Bečvář,[4] F. Belloni,[9] E. Berthoumieux,[9] J. Billowes,[10] V. Boccone,[11] D. Bosnar,[12] M. Brugger,[11] M. Calviani,[11] F. Calviño,[13] C. Carrapiço,[14] F. Cerutti,[11] E. Chiaveri,[11,9] M. Chin,[11] N. Colonna,[8] G. Cortés,[13] M. A. Cortés-Giraldo,[15] M. Diakaki,[16] C. Domingo-Pardo,[17] R. Dressler,[18] I. Durán,[19] C. Eleftheriadis,[20] A. Ferrari,[11] K. Fraval,[9] V. Furman,[21] K. Göbel,[5] M. B. Gómez-Hornillos,[13] S. Ganesan,[22] A. R. García,[2] G. Giubrone,[17] I. F. Gonçalves,[14] A. Goverdovski,[23] E. Griesmayer,[24] C. Guerrero,[11,15] F. Gunsing,[9] T. Heftrich,[5] A. Hernández-Prieto,[11,13] J. Heyse,[25] D. G. Jenkins,[26] E. Jericha,[24] F. Käppeler,[27] Y. Kadi,[11] D. Karadimos,[16] T. Katabuchi,[28] V. Ketlerov,[23] V. Khryachkov,[23] N. Kivel,[18] P. Koehler,[29] M. Kokkoris,[16] J. Kroll,[4] C. Lampoudis,[9] C. Langer,[5] E. Leal-Cidoncha,[19] C. Lederer,[30] H. Leeb,[24] L. S. Leong,[7] J. Lerendegui-Marco,[15] R. Losito,[11] A. Mallick,[22] A. Manousos,[20] J. Marganiec,[6] T. Martínez,[2] C. Massimi,[31,32] P. Mastinu,[33] M. Mastromarco,[8] A. Mengoni,[34] P. M. Milazzo,[35] F. Mingrone,[31] M. Mirea,[36] W. Mondelaers,[25] C. Paradela,[19] A. Pavlik,[30] J. Perkowski,[6] A. J. M. Plompen,[25] J. Praena,[15] J. M. Quesada,[15] T. Rauscher,[37] R. Reifarth,[5] A. Riego-Perez,[13] M. Robles,[19] C. Rubbia,[11] J. A. Ryan,[10] M. Sabaté-Gilarte,[11,15] R. Sarmento,[14] A. Saxena,[22] P. Schillebeeckx,[25] S. Schmidt,[5] D. Schumann,[18] P. Sedyshev,[21] G. Tagliente,[8] J. L. Tain,[17] A. Tarifeño-Saldivia,[17] D. Tarrío,[19] L. Tassan-Got,[7] A. Tsinganis,[11] S. Valenta,[4] G. Vannini,[31,32] V. Variale,[8] P. Vaz,[14] A. Ventura,[31] M. J. Vermeulen,[26] V. Vlachoudis,[11] R. Vlastou,[16] A. Wallner,[38] T. Ware,[10] M. Weigand,[5] C. Weiss,[24] T. Wright,[10] and P. Žugec[12]

(n_TOF Collaboration)

[1]*CIEMAT, Centro de Investigaciones Energéticas Medioambientales y Tecnológicas, Madrid, Spain*
[2]*Centro de Investigaciones Energéticas Medioambientales y Tecnológicas (CIEMAT), Spain*
[3]*NAPC-Nuclear Data Section, International Atomic Energy Agency (IAEA), Vienna, Austria*
[4]*Charles University, Prague, Czech Republic*
[5]*Goethe University Frankfurt, Germany*
[6]*University of Lodz, Poland*
[7]*Institut de Physique Nucléaire, CNRS-IN2P3, Université Paris-Sud, Université Paris-Saclay, F-91406 Orsay Cedex, France*
[8]*Istituto Nazionale di Fisica Nucleare, Sezione di Bari, Italy*
[9]*CEA Saclay, Irfu, Gif-sur-Yvette, France*
[10]*University of Manchester, United Kingdom*
[11]*European Organization for Nuclear Research (CERN), Switzerland*
[12]*Department of Physics, Faculty of Science, University of Zagreb, Croatia*
[13]*Universitat Politècnica de Catalunya, Spain*
[14]*Instituto Superior Técnico, Lisbon, Portugal*
[15]*Universidad de Sevilla, Spain*
[16]*National Technical University of Athens, Greece*
[17]*Instituto de Física Corpuscular, Universidad de Valencia, Spain*
[18]*Paul Scherrer Institut (PSI), Villigen, Switzerland*
[19]*University of Santiago de Compostela, Spain*
[20]*Aristotle University of Thessaloniki, Thessaloniki, Greece*
[21]*Joint Institute for Nuclear Research (JINR), Dubna, Russia*
[22]*Bhabha Atomic Research Centre (BARC), India*
[23]*Institute of Physics and Power Engineering (IPPE), Obninsk, Russia*
[24]*Technische Universität Wien, Austria*
[25]*European Commission, Joint Research Centre, Geel, Retieseweg 111, B-2440 Geel, Belgium*
[26]*University of York, United Kingdom*
[27]*Karlsruhe Institute of Technology, Campus North, IKP, 76021 Karlsruhe, Germany*
[28]*Tokyo Institute of Technology, Japan*
[29]*Oak Ridge National Laboratory (ORNL), Oak Ridge, Tennessee 37831, USA*
[30]*University of Vienna, Faculty of Physics, Vienna, Austria*
[31]*Istituto Nazionale di Fisica Nucleare, Sezione di Bologna, Italy*
[32]*Dipartimento di Fisica e Astronomia, Università di Bologna, Italy*
[33]*Istituto Nazionale di Fisica Nucleare, Sezione di Legnaro, Italy*
[34]*Agenzia nazionale per le nuove tecnologie (ENEA), Bologna, Italy*
[35]*Istituto Nazionale di Fisica Nucleare, Sezione di Trieste, Italy*

*emilio.mendoza@ciemat.es

[36]*Horia Hulubei National Institute of Physics and Nuclear Engineering, Romania*
[37]*Department of Physics, University of Basel, Switzerland*
[38]*Australian National University, Canberra, Australia*

We measured the neutron capture-to-fission cross-section ratio (α ratio) and the capture cross section of ^{235}U between 0.2 and 200 eV at the n_TOF facility at CERN. The simultaneous measurement of neutron-induced capture and fission rates was performed by means of the n_TOF BaF$_2$ Total Absorption Calorimeter (TAC), used for detection of γ rays, in combination with a set of micromegas detectors used as fission tagging detectors. The energy dependence of the capture cross section was obtained with help of the ^{6}Li(n, t) standard reaction determining the n_TOF neutron fluence; the well-known integral of the ^{235}U(n, f) cross section between 7.8 and 11 eV was then used for its absolute normalization. The α ratio, obtained with slightly higher statistical fluctuations, was determined directly, without need for any reference cross section. To perform the analysis of this measurement we developed a new methodology to correct the experimentally observed effect that the probabilities of detecting a fission reaction in the TAC and the micromegas detectors are not independent. The results of this work have been used in a new evaluation of ^{235}U performed within the scope of the Collaborative International Evaluated Library Organisation (CIELO) Project, and are consistent with the ENDF/B-VIII.0 and JEFF-3.3 capture cross sections below 4 eV and above 100 eV. However, the measured capture cross section is on average 10% larger between 4 and 100 eV.

I. INTRODUCTION

The reduction of the uncertainties on the neutron capture cross section of fissile isotopes plays an essential role for a safer and more economic design of new nuclear systems such as Generation-IV reactors and accelerator driven systems [1–3]. ^{235}U plays a dominant and critical role for the operation of nuclear power plants, and various studies noticed differences in the evaluated capture cross sections and recommended new measurements [4–6].

In recent years, three new measurements have been performed following these recommendations: one of them at CERN, which is the one presented in this work, and two others at Los Alamos National Laboratory by Jandel *et al.* [7] and at the Rensselaer Polytechnic Institute (RPI) by Danon *et al.* [8].

The results of these three experiments have already been incorporated into a new evaluation of ^{235}U performed within the scope of the Collaborative International Evaluated Library Organisation (CIELO) Project, an initiative of the Organisation for Economic Co-operation and Development (OECD)/Nuclear Energy Agency (NEA) Data Bank under Working Party on Evaluation Co-operation (WPEC) Subgroup 40 [9–11] and the IAEA Nuclear Data Section [12]. This evaluation is described in detail in Refs. [11,13,14] and has been adopted by the ENDF/B-VIII.0 library [15].

The measurement of neutron capture cross section for fissile isotopes is challenging due to problems in identification of γ rays from (n, γ) and fission. There are different experimental techniques to tackle this problem. One of them is the γ-ray multiplicity methodology developed in the 1980s [16,17], recently applied by Danon *et al.* [8]. Another is the fission tagging technique [18], used by Jandel *et al.* [7] and in this work.

In this paper we present results on the α-ratio (capture-to-fission cross-section ratio) and capture cross-section measurement of ^{235}U performed at the n_TOF facility at CERN. Both data sets were obtained between 0.2 and 200 eV. In Sec. II we describe the measurement technique. The facility and experimental setup are described in Sec. III, the data reduction analysis in Sec. IV, and the results obtained from this work are shown and compared to the most recent evaluations in Sec. V. Finally, the summary and conclusions are presented in Sec. VI.

II. THE FISSION TAGGING TECHNIQUE

The main idea behind the fission tagging technique is to measure simultaneously the fission and capture reactions by means of charged-particle and γ-ray detectors, respectively. The γ-ray detector is sensitive to both capture and fission reactions, but the charged-particle detector to fission reactions only. By the time coincidence between both detection systems, the prompt fission γ-ray cascades are tagged and subtracted from the experimental capture yield. The methodology was developed originally in the early 1960s at Los Alamos [18] and refurbished in the last years at the Los Alamos Neutron Science Center (LANSCE) [6] and n_TOF [19], with improved setups and detection systems. The isotopes measured recently at LANSCE using this technique are ^{235}U [7], ^{239}Pu [20–22], and ^{242m}Am [23,24], and at n_TOF ^{235}U (the measurement presented in this work; preliminary results can be found in Ref. [25]) and ^{233}U [26].

The neutron cross section for any reaction channel x cannot be measured directly. Instead, the physical observable is the reaction yield, $Y_x(E_n)$, the fraction of incident neutrons inducing the reaction, which is a function of neutron energy E_n. The yield can be expressed (neglecting multiple scattering effects) as a function of the sample thickness n_s, total $\sigma_T(E_n)$ and partial $\sigma_x(E_n)$ cross sections as

$$Y_x(E_n) = \frac{\sigma_x(E_n)}{\sigma_T(E_n)}(1 - e^{-n_s\sigma_T(E_n)}). \quad (1)$$

Experimentally, the reaction yield is determined as

$$Y_x(E_n) = \frac{c_{\text{tot},x}(E_n) - c_{bkg,x}(E_n)}{\varepsilon_x(E_n)\phi_N(E_n)}, \tag{2}$$

where $c_{\text{tot},x}(E_n)$ is the total number of counts registered by the detection system, $c_{bkg,x}(E_n)$ is the sum of the different background components, $\phi_N(E_n)$ is the total number of neutrons impinging on the sample under study, and $\varepsilon_x(E_n)$ is the detection efficiency.

In the fission tagging technique, the subtraction of the prompt fission background in the capture measurement ($x = \gamma$) is performed according to

$$Y_\gamma(E_n) = \frac{c_{tot,\gamma}(E_n) - \frac{c_{tag}(E_n)}{\varepsilon_f^*(E_n)} - c_{oth,\gamma}(E_n)}{\varepsilon_\gamma(E_n)\phi_N(E_n)}, \tag{3}$$

where $c_{tag}(E_n)$ is the number of counts in coincidence between the γ-ray and charged-particle detectors; $\varepsilon_\gamma(E_n)$ is the capture detection efficiency; $\varepsilon_f^*(E_n)$, hereafter referred to as *fission tagging detection efficiency*, is the fraction of counts in the γ-ray detector due to prompt fission which have been detected in coincidence with the charged-particle detector; and $c_{oth,\gamma}(E_n)$ is the sum of the remaining background components.

The variables $c_{tot,\gamma}(E_n)$ and $c_{tag}(E_n)$ are not independent. To avoid this and propagate uncertainties in a simpler way, Eq. (3) can be rewritten as

$$Y_\gamma = \frac{c_{aco,\gamma} - \frac{1-\varepsilon_f^*}{\varepsilon_f^*}c_{tag} - c_{oth,\gamma}}{\varepsilon_\gamma \phi_N}, \tag{4}$$

where all the variables depend in principle on the neutron energy E_n, although it is not shown explicitly. Here $c_{aco,\gamma}(E_n)$ is the number of counts in the γ-ray detector not in coincidence with the charged-particle detector, so $c_{tot,\gamma}(E_n) = c_{aco,\gamma}(E_n) + c_{tag}(E_n)$.

From the previous expressions it follows that the ratio between the capture and fission ($x = f$) cross sections, the α ratio $\alpha(E_n) = \sigma_\gamma(E_n)/\sigma_f(E_n)$, can be obtained experimentally as

$$\alpha = \frac{\varepsilon_f}{\varepsilon_\gamma} \frac{c_{aco,\gamma} - \frac{1-\varepsilon_f^*}{\varepsilon_f^*}c_{tag} - c_{oth,\gamma}}{c_{aco,f} + c_{tag} - c_{bkg,f}}, \tag{5}$$

where, again, the dependency of the variables with the neutron energy is not shown explicitly. ε_f is the fission detection efficiency of the charged-particle detector and $c_{aco,f}(E_n)$ is, similarly to $c_{aco,\gamma}(E_n)$, the number of counts in the charged-particle detector not in coincidence with the γ-ray detector. In Eq. (5) the α ratio does not depend on the sample characteristics (mass, inhomogeneities, etc.) or the neutron fluence (absolute value and energy dependency), thus minimizing systematic uncertainties.

Equation (5) is valid for fixed neutron energies. In practice, experimental quantities are always integrated in energy bins. As a consequence, the dependence on the characteristics of the sample and on the energy dependence of the neutron fluence are not completely removed. However, this dependence is very small if the integration bins are narrow. The dependence on the absolute value of the neutron fluence is removed in any case.

In an experiment performed using the fission tagging technique, three quantities are being measured simultaneously: the capture yield, the fission yield, and the ratio between them. The fission cross section is obtained from Eq. (2), the capture cross section from Eq. (4), and the α ratio from Eq. (5). In principle, the capture cross section could also be obtained from the measured α ratio multiplied by a well-known fission cross section. This second option, not used in this work, could provide smaller uncertainties due to systematic effects associated with the sample and neutron fluence characteristics, but, however, will provide larger uncertainties due to counting statistics.

There are some difficulties inherent in the fission tagging technique: (i) the large amount of structural material intercepting the neutron beam due to the charged-particle detector which could produce a large amount of background in the γ-ray detection system, (ii) the low counting statistics due to the use of very thin targets required for high fission detection efficiency, and (iii) the systematic uncertainties associated with the detection efficiencies. Regarding case (iii), the contribution to the overall uncertainty of ε_f^* could become very important when fission dominates over capture. If we consider that $\varepsilon_f = \varepsilon_f^*$ and ε_f^* does not vary with the neutron energy, and we neglect the background components not related to fission, then the propagation of the uncertainty in ε_f^*, $\Delta\varepsilon_f^*$, in the capture yield and the α ratio is

$$\frac{\Delta Y_\gamma(E_n)|_{\varepsilon_f^*}}{Y_\gamma(E_n)} \simeq \left(\frac{\sigma_f(E_n)}{\sigma_\gamma(E_n)}\frac{\varepsilon_F}{\varepsilon_\gamma}\right)\frac{\Delta\varepsilon_f^*}{\varepsilon_f^*}, \tag{6}$$

$$\frac{\Delta\alpha(E_n)|_{\varepsilon_f^*}}{\alpha(E_n)} \simeq \left(1 + \frac{\sigma_f(E_n)}{\sigma_\gamma(E_n)}\frac{\varepsilon_F}{\varepsilon_\gamma}\right)\frac{\Delta\varepsilon_f^*}{\varepsilon_f^*}, \tag{7}$$

where ε_F is the probability of detecting a fission reaction in the γ-ray detector. Therefore, if fission dominates over capture, having a low uncertainty in ε_f^* is crucial, unless the γ-ray detector is able to differentiate fission from capture effectively ($\varepsilon_\gamma \gg \varepsilon_F$).

If the probability of detecting a fission reaction in one of the two detectors (γ-ray or charged-particle) does not depend on whether or not it was detected in the other detector, then $\varepsilon_f^*(E_n) = \varepsilon_f(E_n)$; i.e., the fission tagging detection efficiency is equal to the fission detector efficiency. However, in general $\varepsilon_f^*(E_n) \neq \varepsilon_f(E_n)$.

Due to the aforementioned difficulties, not all the charged-particle and γ-ray detectors are suitable for this technique. Before performing the experiment described in this paper, a test was carried out at n_TOF to study the feasibility of our detection system [19], which consists of the n_TOF BaF$_2$ Total Absorption Calorimeter (TAC) [27] as a γ-ray detector, and micromegas detectors [28] as charged-particle detectors.

III. THE EXPERIMENTAL SETUP

A. The n_TOF facility at CERN

n_TOF [29–31] is a time-of-flight facility based on proton pulses of 6 ns width and 20 GeV/c momentum delivered by the CERN Proton Synchrotron (PS). The pulses, with a nominal intensity of 7×10^{12} protons per pulse, impact on a lead

spallation target, yielding about 300 fast neutrons per incident proton. A layer of water around the lead target moderates the neutrons produced in spallation reactions resulting in a white spectrum in the full range of energies between meV and GeV [32].

The neutrons travel from the spallation target to the experimental areas where their energy is determined by the time-of-flight technique. The ^{235}U(n, γ) experiment was carried out in EAR-1, the horizontal beam line situated at 185 m from the target. Here the high instantaneous neutron intensity and wide energy range combined with the state-of-the-art detectors have provided a large number of high-quality neutron-induced cross-section measurements in the last two decades [33].

During the ^{235}U(n, γ) experiment, three different detectors were used for monitoring the beam: the wall current monitor (WCM) [30] and the beam current transformer (BCT) [30], focused on the proton beam control; and the silicon flux monitor (SiMon) [34], based on the ^{6}Li(n, t) standard reaction, which monitored the incident neutron beam. The latter was also used to obtain the energy dependence of the neutron fluence during the measurement.

B. The Total Absorption Calorimeter

The TAC [27] is an array made of 40 BaF$_2$ detectors covering almost the 4π solid angle. The detector was specifically designed for detecting the γ-ray cascades emitted in the (n, γ) process.

The BaF$_2$ crystals, with pentagonal and hexagonal shapes enclosed in ^{10}B enriched carbon fiber capsules, form a spherical shell of 21- and 51-cm inner and outer diameters, respectively. Each individual BaF$_2$ crystal is coupled to a Photonis XP4508B photomultiplier and a voltage divider specifically designed for its fast recovery. The assembly is housed in an aluminum cover with a magnetic shield to protect the charge recollection in the photomultiplier. A schematic picture of the TAC is shown in Fig. 1.

The nearly 100% detection efficiency of the TAC together with the high n_TOF instantaneous neutron fluence allows measurements with small mass and/or radioactive samples.

C. The Fission Tagging MicromeGas detectors

The Fission Tagging MicromeGas (FTMG) detectors [28,35,36] are gaseous parallel plate detectors equipped with three electrodes: cathode, micromesh, and anode. The active volume of the detector is separated into two regions: the drift gap, between the cathode and the micromesh, and the amplification gap, situated in the region between the micromesh and the anode plate. The sample is placed close to the cathode. The ionization of the gas induced by the fission fragments produces electrons that are accelerated in the drift gap, with an electric field of ≈ 1 kV/cm, until reaching the micromesh. Between the micromesh and the anode, a narrow amplification space with ≈ 50 kV/cm produces the multiplication of the incoming charge by an avalanche process. The detectors, with 60 mm in diameter, 8.1 mm drift gap, and 40 μm amplification gap, were specifically designed to fit inside a small sealed
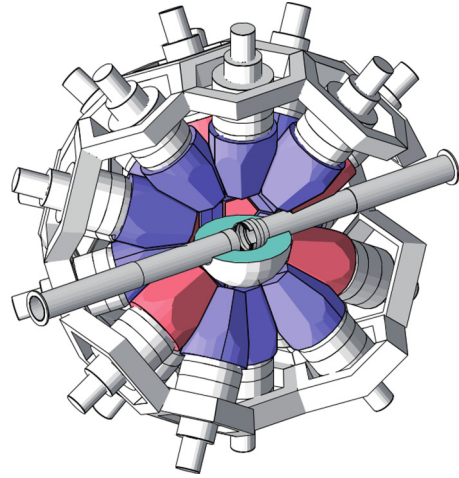

FIG. 1. Schematic view of part of the n_TOF TAC, together with beam pipes and half of a neutron absorber inside (not the one used in this measurement). Some of the BaF$_2$ modules are not shown, to make it possible to see the center. BaF$_2$ crystals with pentagonal and hexagonal shapes appear, respectively, in red and blue.

fission chamber covering the entire neutron beam profile. A picture of the FTMG detectors is shown in Fig. 2.

The FTMG detectors were operated with a premixed gas mixture of Ar + (10%)CF$_4$ + (2%)iC$_4$H$_{10}$ at atmospheric pressure (1 bar) and placed together with the ^{235}U samples inside the sealed fission chamber in the center of the TAC. The fission chamber is 63 mm in diameter and 150 mm in length. To shield the TAC from the neutrons scattered by the material directly placed into the beam, the chamber was surrounded by a 5-cm-thick spherical borated polyethylene neutron absorber as it is displayed in Fig. 3.

D. Data acquisition system and event reconstruction

The signals from the individual detectors were recorded by the front-end n_TOF digital acquisition system (DAQ) [37] based on Acquiris-DC270 digitizers with 8-bit resolution and 8 MB memory. The acquisition sampling rate was chosen for the individual detectors according to their specific signal bandwidth: 250 Msamples/s for the BaF$_2$ detectors and 100 Msamples/s for the FTMG and the SiMon detectors. The DAQ allowed to record continuously a 32 ms pulse, which
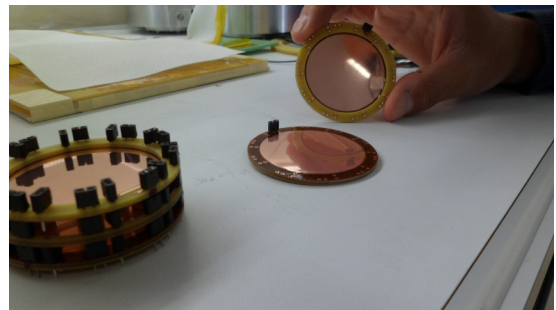

FIG. 2. Picture of the FTMG detectors used during the ^{235}U(n, γ) campaign.
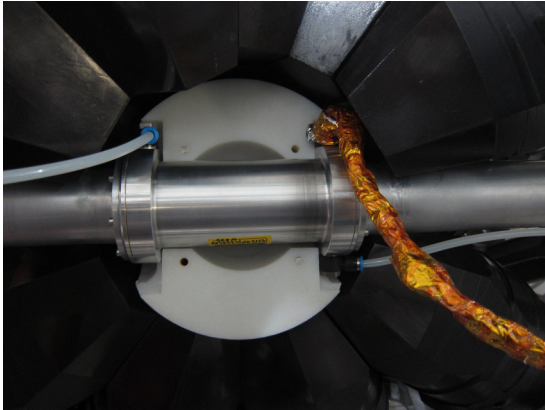
FIG. 3. Picture of the fission chamber placed in the center of the TAC. In white, half of the borated polyethylene neutron absorber shell.

allowed to determine the capture cross section and α ratio down to a neutron energy of 0.2 eV.

The raw signals were analyzed offline by dedicated pulse shape reconstruction routines [38,39]. For each analyzed BaF_2 signal, the reconstruction algorithm returns the associated time-of-flight, signal amplitude, signal integrals corresponding to the fast and slow scintillation components, and module number. These individual detector signals, calibrated in deposited energy, are grouped using a coincidence window of 20 ns providing TAC events characterized by their total deposited energy, E_{sum}, crystal multiplicity, m_{cr} (number of detectors in coincidence contributing to the event), and time of flight. For the SiMon and the FTMG detectors, the reconstruction algorithm characterizes the events by their associated time of flight, signal amplitude, and module number.

E. The ^{235}U targets, experimental setup, and dedicated measurements

The measurement campaign was performed with 41.15(5) mg of ^{235}U, distributed into ten isotopically enriched samples of ^{235}U$_3$O$_8$ (^{233}U, <0.001%; ^{234}U, 0.036%; ^{235}U, 99.934%; ^{236}U, 0.010%; ^{238}U, 0.021%) manufactured by the Joint Research Center-Geel. The radioactive material was electrodeposited on 20-μm-thick and 42-mm-diam aluminum backings, yielding a surface density of $\approx$300 μg/cm^2 per sample [40]. The amount of ^{235}U was not the same in all the samples, with differences of up to 25% between them.

After some tests it was found that the size of the background induced in the TAC by the FTMG detectors was very high and a configuration with less FTMG detectors than uranium targets was preferred. For this reason, the measurement was performed with the targets distributed in eight bare samples and the remaining two encapsulated back-to-back into two FTMG detectors. Despite of the low TAC-FTMG expected coincidence efficiency for fission events ($\approx$20%), this configuration was preferred to reduce the background associated with the material intercepting the neutron beam.

The measurement was carried out over 4 months, from the end of June up to the end of October 2012, with a total number

of $\approx$4.0 $\times$ 10^{18} protons delivered to the spallation target. Part of the beam time was dedicated to determine the background, by measuring dummy samples inside the fission chamber. Although the majority of the time-of-flight spectra were obtained from measurements with the borated polyethylene neutron absorber in place, a fraction of the beam time was dedicated to measurements without the neutron absorber as well, in order to register a cleaner detector response to the (n, γ) cascades (see Sec. IV E). The temperature of the experimental area, which was monitored continuously, was 297 $\pm$ 2 K.

Periodic energy calibrations of the BaF_2 detectors were performed with standard γ-ray calibration sources: ^{137}Cs, ^{88}Y, and Am/Be. In addition, the gains of the BaF_2 detectors were monitored continuously using the α decay of Ra impurities in the crystals.

IV. DATA REDUCTION

We calculated the capture cross section and the α ratio according to Eqs. (4) and (5), respectively. For the capture cross section we used the thin target approximation; i.e., we assumed that $Y_x(E_n) \simeq n_s\sigma_x(E_n)$. This approximation is fully justified throughout the entire range of the measurement, since the self-shielding in our sample, with a total thickness of 7.6×10^{-6} atoms/b, is negligible. It allows one to use the well-known integral of the ^{235}U(n, f) cross section from 7.8 to 11 eV to normalize the capture data. With this normalization the result no longer depends on the mass of the sample or the absolute value of the neutron fluence.

In this section we describe in detail how the different quantities appearing in Eqs. (4) and (5) have been obtained. Other analyses performed with the TAC, although without fission tagging detectors, can be found in Refs. [41–45], and the previous test with fission tagging in Ref. [19].

A. FTMG detectors

The background in the FTMG detectors, $c_{bkg,f}(E_n)$, was efficiently suppressed by selecting an amplitude threshold A_{th} high enough to avoid the detection of the α particles from the natural decay of ^{235}U. The detection efficiency $\varepsilon_f(E_n)$ is not expected to vary in the energy range of our measurement and is considered to be constant.

To validate the performance of the FTMG detectors, we verified that the measured fission cross section is very similar to those in evaluations. It was obtained from Eq. (2) and normalized, similarly to the capture cross section, to the well-known integral of the ^{235}U(n, f) cross section from 7.8 to 11 eV. As an example, we show the comparison with JEFF-3.3 [46,47] in Fig. 4. Recent fission measurements at n_TOF show a similar level of agreement [48]. The fission cross section obtained in this work is also compared with other evaluations in Sec. V B.

B. Background in the TAC

There are different sources of background in the TAC, which can be classified as follows: (i) events not related with the neutron beam, coming from internal radioactive decay of the BaF_2 crystals, environmental background, and natural
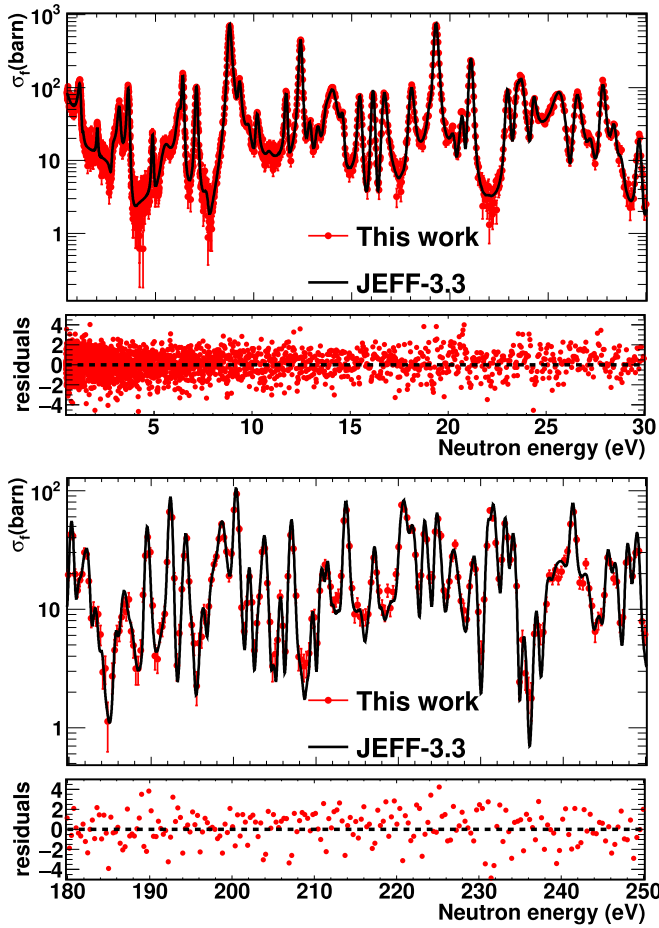
FIG. 4. Fission cross section obtained with the FTMG detectors (this work) compared with JEFF-3.3, in two different neutron energy ranges. The residuals correspond to the difference between the measured and the evaluated cross sections divided by the uncertainty due to counting statistics.

FIG. 5. Total deposited energy registered by the TAC, in anticoincidence with the FTMG detectors, during the ^{235}U(n, γ) measurement (Total), together with different contributions to the total spectrum (see the text for details). The data correspond to neutron energies between 1 and 20 eV and $m_{cr} > 2$. The full capture Q peak is broadened due to the presence of the neutron absorber and a long-lived isomeric state of ^{236}U.

decay of the ^{235}U targets; (ii) events related with the interaction of the neutron beam with materials different from the ^{235}U targets; (iii) prompt fission background, i.e., events coming from neutron-induced fission reactions in ^{235}U which are detected within the used coincidence window; and (iv) other components related to the ^{235}U targets: elastic scattering, delayed detection of prompt fission neutrons, and fission fragment decay.

Components (i) and (ii) were obtained from dedicated measurements, in particular, (i) by measuring without neutron beam and (ii) by replacing the ^{235}U targets with dummy samples. Component (iii) was determined from the time coincidences between the TAC and the FTMG detectors. For that, the number of events detected in coincidence $c_{tag}(E_n)$ has been rescaled by a factor $\frac{1 - \varepsilon_f^*}{\varepsilon_f^*}$ according to Eqs. (4) and (5). The last component (iv), much smaller than the previous ones, has been determined by Monte Carlo simulations [49].

In Fig. 5 we show several total deposited energy spectra in the TAC, all of them corresponding to neutrons between 1 and 20 eV and for $m_{cr} > 2$ conditions. The one labeled
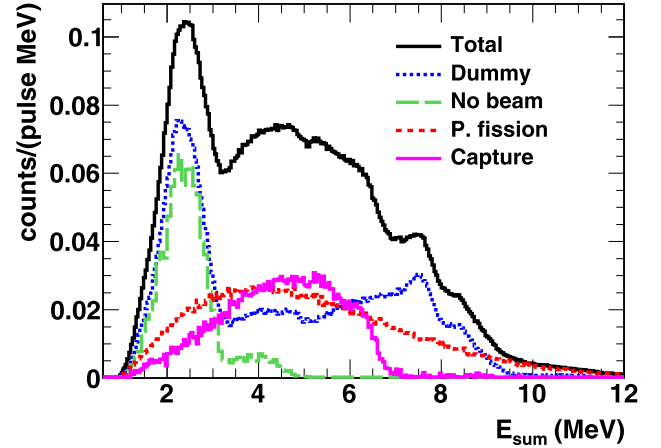
"Total" corresponds to that measured with neutron beam and the ^{235}U samples, in anticoincidence with the FTMG detectors [$c_{aco,\gamma}$ in Eqs. (4) and (5)]. The spectra labeled "Dummy" and "No beam" correspond, respectively, to the results of the measurements performed with beam and the dummy samples, and without neutron beam. The prompt fission background contribution, i.e., component (iii), is labeled "P. fission" and the spectrum due to (n, γ) reactions is labeled "Capture."

We have selected certain analysis conditions on the detected events in order to improve the capture-to-background ratio, but without reducing too much the capture detection efficiency. We have sought a compromise between both these requirements. Figure 5 shows that the capture-to-background ratio is significantly improved if the high ($E_{sum} > 7$ MeV) energy events are excluded from the analysis, without affecting the detection of capture cascades, since $S_n(n + ^{235}$U$) = 6.5$ MeV. Furthermore, capture events have higher average multiplicity m_{cr} than some of the nonfission background components, but lower than fission events. A detailed check of various cuts shows that the smallest uncertainty was obtained if TAC events with $2.5 < E_{sum} < 7.0$ and $2 < m_{cr} < 6$ were considered, which have been adopted in the present analysis.

The numbers of counts per proton pulse using these cuts are presented in Figs. 6 and 7, as a function of neutron energy. "Total" corresponds to all the events detected in anticoincidence with the FTMG detectors in the ^{235}U(n, γ) measurement. Figure 6 also shows the results of the measurements with the dummy samples (Dummy) and without neutron beam (No beam), together with prompt (P) fission—background component (iii)—and delayed (D) fission—dominant contribution to background component (iv).

In principle, component (ii) of the background should be easily obtained from the measurement with dummy samples. However, when studying the different deposited energy
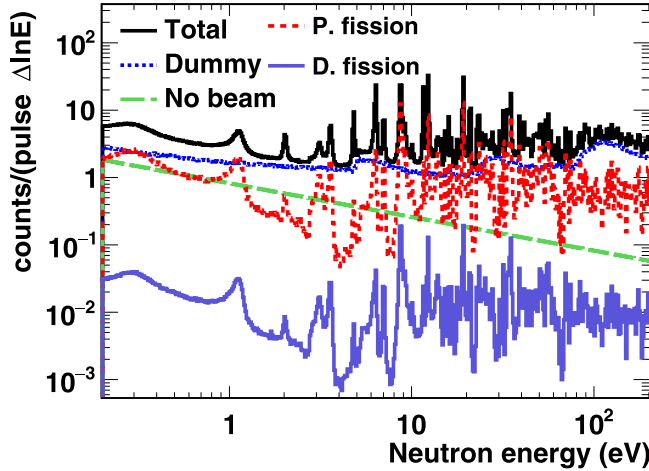
FIG. 6. Number of events detected in the TAC in anticoincidence with the FTMG detectors in the ^{235}U(n, γ) measurement (Total) per pulse and per unit lethargy ($\Delta \ln E$, which means that the bin contents have been divided by the natural logarithm of the ratio between the upper and lower bin limits) as a function of neutron energy, together with different background components. Only events with $2 < m_{cr} < 6$ and $2.5 < E_{sum} < 7$ MeV are considered.

spectra we observed that the amount of counts due to this background component was slightly higher in the measurement with dummy than with ^{235}U targets. This effect increases with neutron energy, being negligible below 20 eV. After a detailed study we have concluded that this effect is due to the fact that the borated polyethylene neutron absorber shell was not placed in exactly the same position in both measurements [49].

We therefore scaled the measured background to fit the total deposited energy spectrum (see Fig. 5) above 7 MeV. We estimated the uncertainty due to this correction, and propa-
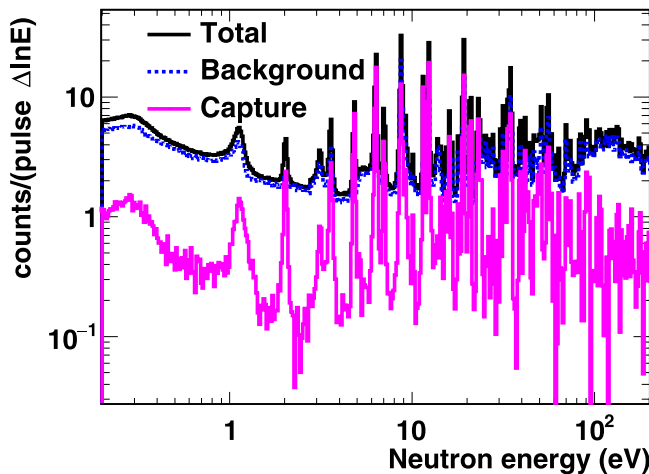

FIG. 7. Number of events detected in the TAC in anticoincidence with the FTMG detectors in the ^{235}U(n, γ) measurement (Total) per pulse and per unit lethargy as a function of neutron energy (same as in Fig. 6), together with the total background (Background) and the counts due to ^{235}U(n, γ) reactions (Capture).
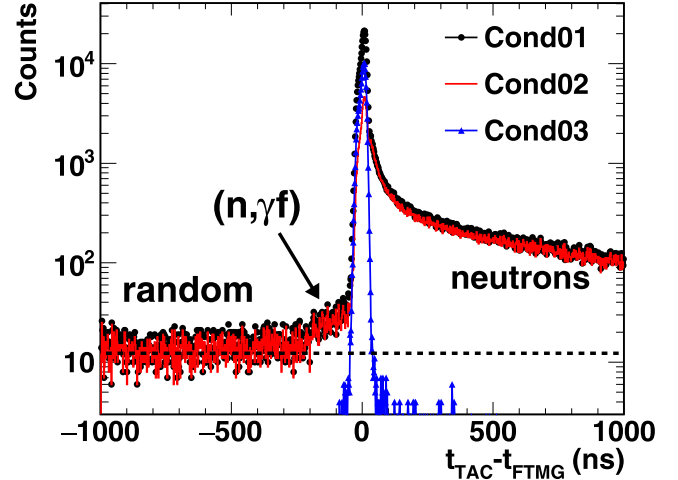

FIG. 8. Time difference distribution between events from the TAC and the FTMG detectors, for times of flight corresponding to neutron energies between 0.2 and 1.2 eV. Three different cuts in the TAC events were considered: no cuts (Cond01); $E_{sum} < 2.5$ MeV and $m_{cr} \leqslant 4$ (Cond02); and $E_{sum} > 2.5$ MeV and $m_{cr} > 4$ (Cond03). The dotted line is the estimate of random coincidences.

gated it to the final results as shown in Sec. V. Both the scaling factor and its uncertainty depend on the neutron energy. The scaling factor deviates from unity by less than 7% in the entire range, and its uncertainty by less than 2%.

The total background, obtained after adding all the components and after taking into account the mentioned corrections, is presented in Fig. 7.

C. TAC-FTMG time-coincidence analysis

Figure 8 shows time differences between the TAC and the FTMG detectors, $t_{TAC} - t_{FTMG}$, from neutron energies 0.2–1.2 eV for three different cuts on E_{sum} and m_{cr} as specified in the caption. Cond01 corresponds to no conditions at all, and Cond02 and Cond03 to TAC events with low and high E_{sum} and m_{cr}, respectively. Cond03 corresponds almost entirely only to the detection of prompt fission γ-ray cascades.

The time distribution presented in Fig. 8 is formed by the following effects:

(i)   The random coincidences, the level of which can be deduced from negative times (below about 500 ns), are indicated in the figure by the horizontal dotted line.

(ii) Prompt fission γ-rays in the TAC form a peak near zero time difference.

(iii) Delayed detection of fission reactions can occur at later times in the TAC, due to prompt fission neutrons undergoing an interaction in or near the TAC producing γ rays, or due to fission fragments decay (β, βn, or isomeric). These events contribute to the tail at positive time differences.

(iv) The $(n, \gamma f)$ events [50–52] form an exponential tail visible for time differences between -200 and -50 ns.

TABLE I. $(n, \gamma f)/(n, f)$ ratio and isomer's half-life deduced from the TAC-FTMG time-coincidence distribution. Uncertainties, in parentheses, are due to counting statistics. The values obtained in this work are compared to those provided in Refs. [53,54].

Ref.	E_n	$t_{1/2}$ (ns)	$(n, \gamma f)/(n, f)$ (%)
This work	0.2–1.2 eV	68(6)	0.066(6)
This work	1.2–12.0 eV	66(3)	0.125(18)
[53]		120(2)	
[54]	2.2 MeV	66.6(87)	0.031

Virtually all high E_{sum} and high m_{cr} events in the TAC (Cond03) are grouped around zero, as expected since they correspond to prompt fission γ-ray cascades. From this distribution we have chosen the TAC-FTMG coincidence time window. Two opposite criteria have been considered: include as much as possible the prompt fission events, and minimize the random coincidences. The optimum interval was found to be between -50 and 30 ns, which covers virtually all the Cond03 events.

Monte Carlo simulations show that the tail for positive time differences is dominated by the detection of the prompt fission neutrons, and the contribution of the fission fragments decay is significantly smaller. The detection of the prompt fission neutrons occurs mainly through three processes: inelastic scattering in the BaF_2, (n, α) reactions in the ^{10}B of the absorber or the crystals' carbon fiber capsules, and capture reactions in the BaF_2. The first process takes place in the first few nanoseconds after the fission, and is detected in coincidence with the prompt fission γ-ray cascade. The second process takes place after the neutron is moderated in the absorbent, so it extends to longer times, and is the main contributor to the tail visible in Fig. 8. Since (n, α) reactions in boron produce a 478-keV γ ray, most of the TAC events in this tail have low E_{sum} and low m_{cr} and are thus removed by application of cuts used in the analysis. The contribution of the third process is much smaller than that of the other two.

Concerning the $(n, \gamma f)$ events (iv), the compound nucleus first decays via γ-ray emission until reaching another (intermediate) excited state of ^{236}U, which then decays via fission as an alternative to γ-ray emission. If the intermediate excited state has a sufficiently long half-life, then it is possible to differentiate in time the detection of the first γ-ray cascade by the TAC from the detection of the subsequent fission fragments by the FTMG detectors. By fitting the exponential tail corresponding to $(n, \gamma f)$ reactions we have obtained the half-life of the intermediate state and, taking into account different detection efficiencies, also the $(n, \gamma f)/(n, f)$ ratio. These quantities for two incident neutron energy intervals are given in Table I.

The same half-life deduced from different neutron energies indicates that there is only one excited state undergoing this (delayed) fission. A very good candidate for this state is the one at 2.750 MeV, which is supposed to be the ground state in the second potential well [53]. The evaluated half-life of this level in Ref. [53] is 120(2) ns, but there are many other reported values, some of them very different from the

evaluated one. One of them, with 66.6(87) ns [54], obtained from 2.2 MeV neutron-induced fission reactions on ^{235}U, seems to be in good agreement with our value. As the total deposited energy in the TAC before the fission, which should come from the (n, γ) reaction, is 3–4 MeV, the state should really have an excitation energy close to 2.5 MeV, since $S_n(n + {}^{235}U) = 6.5$ MeV.

Application of $2.5 < E_{\text{sum}} < 7$ MeV and $2 < m_{cr} < 6$ cuts significantly eliminates events from $(n, \gamma f)$ as they have $m_{cr} \leqslant 2$. A similar situation happens also for random coincidences, since most of the events in the TAC have low E_{sum} and low m_{cr}. As a result, almost exclusively only prompt fission events are thus considered in the analysis.

D. The fission and fission tagging detection efficiencies

In this work we use the following efficiencies, which are assumed to be constant in the energy range of this measurement:

(a) ε_f is the fission efficiency, defined as the probability of detecting a fission reaction induced in any of the ten ^{235}U samples with the FTMG detectors. It depends only on the amplitude thresholds A_{th} applied to the FTMG detectors, $\varepsilon_f = \varepsilon_f(A_{th})$.

(b) ε_f^* is the fission tagging detection efficiency, defined as the fraction of counts in the TAC due to prompt fission which have been detected in coincidence with the FTMG detectors. It depends, in principle, on A_{th} and also on the cuts in E_{sum} and m_{cr} applied to the TAC events, $\varepsilon_f^* = \varepsilon_f^*(A_{th}, E_{\text{sum}}, m_{cr})$.

(c) ε_F is the probability of detecting a prompt fission reaction in the TAC. It depends on the cuts in E_{sum} and m_{cr}, $\varepsilon_F = \varepsilon_F(E_{\text{sum}}, m_{cr})$.

As shown in Eqs. (4) and (5), we need to calculate $\varepsilon_f(A_{th})$ and $\varepsilon_f^*(A_{th}, E_{\text{sum}}, m_{cr})$, for the A_{th}, E_{sum}, and m_{cr} cuts used in the analysis, which is not straightforward. We can obtain ε_f^* experimentally by dividing the number of counts in coincidence, c_{tag}, by the number of counts in the TAC due to prompt fission, $c_{fis,\gamma}$,

$$\varepsilon_f^*(A_{th}, E_{\text{sum}}, m_{cr}) = \frac{c_{tag}(A_{th}, E_{\text{sum}}, m_{cr})}{c_{fis,\gamma}(E_{\text{sum}}, m_{cr})}, \qquad (8)$$

but $c_{fis,\gamma}$ is not easy to compute accurately if counts due to capture and fission are mixed together. On the contrary, if we select cuts in E_{sum} and m_{cr} which exclude counts due to capture, for example by setting E_{sum} well above the neutron separation energy of ^{236}U, then $c_{fis,\gamma}$ is obtained more easily and accurately by subtracting the background $c_{oth,\gamma}$ from the total counts in the TAC, $c_{tot,\gamma}$.

The more restrictive these cuts are, the less impact the background subtraction has on the result, but the larger are the uncertainties due to counting statistics. We determined ε_f^* for different ^{235}U resonances under different cuts in E_{sum} and m_{cr}, all of them selected to exclude the capture events and to minimize the contribution of the background, i.e., using high E_{sum} and m_{cr} [49]. The results are compatible within uncertainties. For the cuts $E_{\text{sum}} > 10$ MeV and $m_{cr} > 5$, we obtained $\varepsilon_{f,a}^* = 0.1887(15)$, where the subscript a refers to
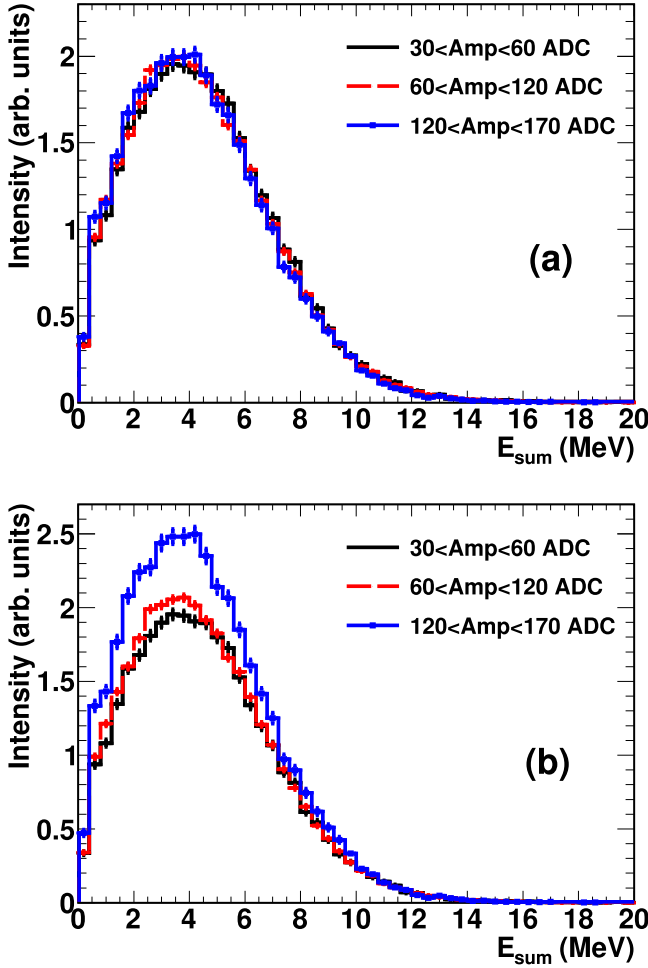
FIG. 9. Total deposited energy spectra in the TAC in coincidence with the FTMG detectors. Each spectrum was constructed by setting different conditions in the FTMG amplitude "Amp," which ranges from 30 to 170 ADC channels. The spectra are normalized to (a) the total area and (b) the $E_{sum} > 10$ MeV region.

these cuts in E_{sum} and m_{cr}. In all the cases we used the A_{th} values used in the analysis.

Provided that the probability of detecting a fission reaction in the TAC or the FTMG detectors does not depend on whether it has been detected in the other detection system, the probability of detecting a fission reaction in coincidence is the product of probabilities, $\varepsilon_F \varepsilon_f$. If this is the case, then $\varepsilon_f^* = (\varepsilon_F \varepsilon_f)/\varepsilon_F = \varepsilon_f$ and ε_f^* depends only on A_{th} and not on the cuts in E_{sum} and m_{cr}.

Although both detection systems are physically independent, there is a correlation between the produced fission fragments and associated prompt γ-ray production [55], including directional correlation [56], and between the fission fragments produced and the number of prompt neutrons emitted [57]. Thereby, depending on the fission fragment detected, slightly different prompt-fission γ rays and neutrons are tagged in the TAC. The detection efficiency in the FTMG detectors is also expected to vary slightly with the fragment mass and with the emitted direction. This effect was experimentally observed as shown in Fig. 9, where three

E_{sum} spectra are displayed, each with different cuts in the FTMG detectors amplitude, Amp, measured in analog-to-digital converter (ADC) channels. Figure 9 shows a slight shift of the spectra to lower energies with increasing Amp. Due to this correlation the shape of the tagged energy spectrum is slightly different from the shape of the total energy spectrum due to fissions. Although this effect is small, its impact on the final result can be large, as Eqs. (6) and (7) show. Therefore, the value of ε_f^* calculated for $E_{sum} > 10$ MeV and $m_{cr} > 5$, $\varepsilon_{f,a}^*$, cannot be directly used for the cuts used in the analysis, and hence some corrections to $\varepsilon_{f,a}^*$ are needed.

The correction we applied in this analysis to the value of $\varepsilon_{f,a}^*$ determined above assumes that (i) the deposited energy spectrum in the TAC corresponding to the fissions not detected by the FTMG detectors is very similar to that of the fissions that deposit little energy in the gas and (ii) the spectra in the TAC due to fissions in each of the samples have the same shape. These assumptions allowed us to obtain the shape of the spectrum in the TAC due to fissions by slightly correcting the shape of the tagged spectrum.

Above we obtained ε_f^* for some cuts $\varepsilon_{f,a}^*(A_{th}) = \varepsilon_f^*(A_{th}, \{E_{sum}, m_{cr}\}_a)$ and we want to calculate it for the cuts used in the analysis, $\varepsilon_{f,b}^*(A_{th}) = \varepsilon_f^*(A_{th}, \{E_{sum}, m_{cr}\}_b)$. Here $\{E_{sum}, m_{cr}\}_a$ means $E_{sum} > 10$ MeV and $m_{cr} > 5$; and $\{E_{sum}, m_{cr}\}_b$ means $2.5 < E_{sum} < 7$ MeV and $2 < m_{cr} < 6$. From Eq. (8) and using the same notation (indices a and b) for c_{tag} and $c_{fis,\gamma}$, the ratio between both ε_f^* values depends on A_{th} as

$$\frac{\varepsilon_{f,a}^*(A_{th})}{\varepsilon_{f,b}^*(A_{th})} = \frac{c_{fis,\gamma,b}}{c_{fis,\gamma,a}} \frac{c_{tag,a}(A_{th})}{c_{tag,b}(A_{th})}, \qquad (9)$$

where the ratio between the $c_{fis,\gamma}$ values does not depend on A_{th} and corresponds to the ratio between type b ($\{E_{sum}, m_{cr}\}_b$) and type a ($\{E_{sum}, m_{cr}\}_a$) contributions to the deposited energy spectrum in the TAC due to prompt fission.

The dependence on A_{th} of the ratio between the c_{tag} values can be obtained experimentally in a broad range of A_{th}. This ratio, for different FTMG signal amplitude intervals, is shown in Fig. 10. Each interval has different widths so that the uncertainties due to counting statistics are similar in all of them. The average of the measured ratios is represented by the horizontal solid line. The amplitude threshold has been extended to lower values than the ones used in the analysis so the detection efficiency of each FTMG detector is $\approx 90\%$. An additional interval, shown inside the shadowed rectangle, represents the 10% fission reactions which have not been detected by the FTMG detectors. According to assumptions (i) and (ii), the $c_{tag,a}/c_{tag,b}$ ratio in this interval is equal to the ratio of the interval with the lowest considered amplitudes. The average ratio taking into account also this interval is represented by the horizontal dashed line.

In the limit where all fissions were detected by the FTMG detectors (corresponding to $A_{th} = 0$), a prompt fission reaction detected in the TAC would be in coincidence with the FTMG detectors if and only if the fission reaction had taken place in a ^{235}U target with the FTMG detector, and so $\varepsilon_{f,a}^*(0) = \varepsilon_{f,b}^*(0) = \varepsilon_f(0)$. Thus, in this limit we obtain the ratio between the $c_{fis,\gamma}$ values, since it is equal to the
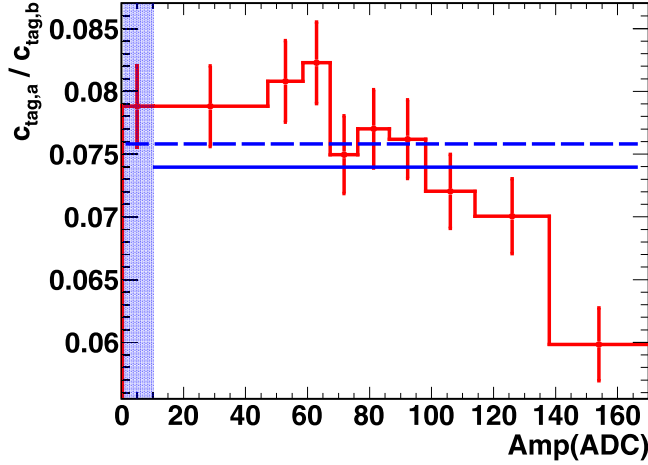
FIG. 10. Ratio between tagged fission events c_{tag} for $\{E_{sum}, m_{cr}\}_a$ and $\{E_{sum}, m_{cr}\}_b$ cuts, for different intervals of the amplitude of the FTMG signals (Amp). The first interval, inside the shadowed rectangle, does not correspond to experimental data. It represents the fissions not detected by the FTMG detectors, and its value is the same as the interval just above the amplitude threshold. The horizontal lines represent the average ratio calculated with (dashed) and without (solid) this first interval. Vertical error bars correspond to uncertainties due to counting statistics.

ratio between the c_{tag} values [Eq. (9)]. With this information, we have obtained $\varepsilon^*_{f,b}(A_{th})$ for the A_{th} used in the analysis (hereafter $\varepsilon^*_{f,b}$).

As a result, we have obtained that $\varepsilon^*_{f,b}$ is 2% lower than $\varepsilon^*_{f,a}$. The uncertainty in this correction has been estimated to be 15%. Thus, the fission tagging detection efficiency for the cuts used in the analysis is $\varepsilon^*_{f,b} = 0.1847(22)$.

Concerning the fission detection efficiency ε_f, we have assumed that it has the same value and uncertainty as $\varepsilon^*_{f,b}$. For the cuts used in the analysis, the efficiency of the TAC to detect fission events ε_F is quite high, contrary to what happens in the case of high E_{sum} and m_{cr} (Fig. 10). For this reason, fission reactions are detected almost independently in both detection systems, and therefore $\varepsilon_f \simeq \varepsilon^*_{f,b}$.

E. The neutron capture detection efficiency

The TAC efficiency for capture events ε_γ was determined by Monte Carlo simulations, similarly to previous works [42,43,45]. The ^{235}U(n, γ) cascades were generated with the DICEBOX code [58], adjusting the parameters of the electromagnetic cascades from the LANSCE experimental ^{235}U(n, γ) data [7]. The same cascades used to reproduce the ^{235}U(n, γ) measurement at LANSCE were then transported into the n_TOF geometry with a code based on the GEANT4 toolkit [59,60]. We added the geometrical model of the compact fission chamber together with the FTMG detectors to the detailed geometry of the TAC implemented for previous analyses [61]. The results of the transport code were then reconstructed as in the real experiment, performing the same type of coincidences, and including all the experimental effects such as the energy resolution of the crystals.
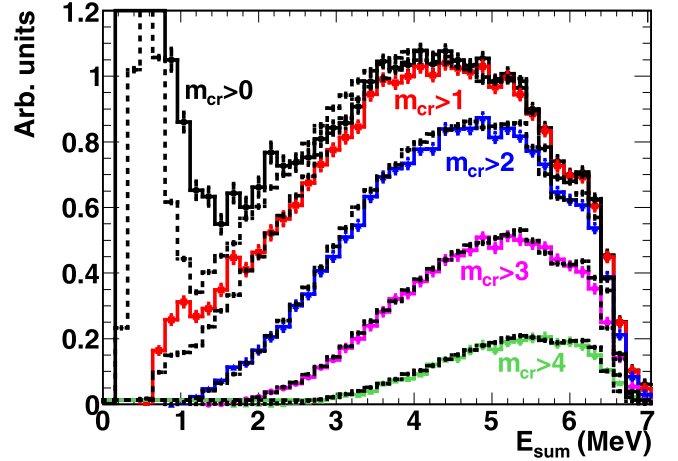

FIG. 11. Experimental (solid lines) and simulated (dotted lines) total deposited energy spectra from ^{235}U(n, γ) cascades for different cuts in m_{cr}, for the geometry with the neutron absorber.

The generated electromagnetic cascades were simulated into two experimental configurations, with and without the neutron absorber shell. The quality of the results is illustrated in Fig. 11 (with absorber) and Fig. 12 (without absorber), where the experimental and simulated total E_{sum} deposited energy spectra, for different m_{cr} cuts, are compared. The excellent agreement between the Monte Carlo simulations and the experimental data above 1.5 MeV permits the determination of the TAC efficiency for the ^{235}U(n, γ) events, which is $\varepsilon_\gamma = 56.5\%$ for the cuts used in the analysis, with an accuracy of 1.7%. The uncertainty was estimated by considering two contributions. The first was the impact of geometry implemented in the Monte Carlo simulation, which was tested by varying the inner radius of the TAC in ± 1 mm. Second, the imperfection of the decay model was obtained from the difference between simulated and experimental spectra.
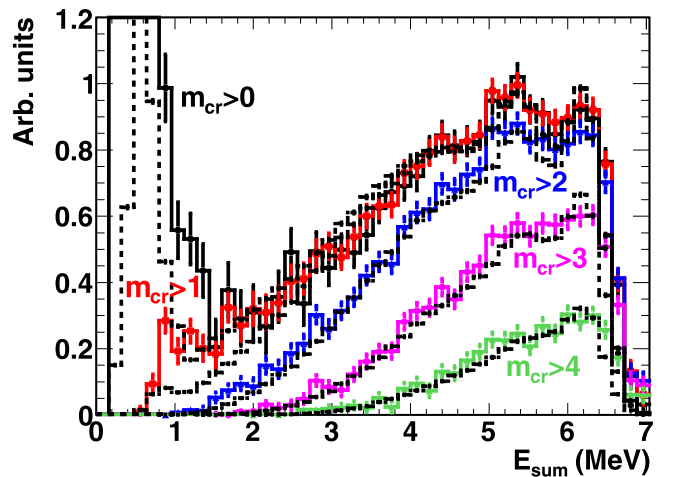

FIG. 12. Experimental (solid lines) and simulated (dotted lines) total deposited energy spectra from ^{235}U(n, γ) cascades for different cuts in m_{cr}, for the geometry without the neutron absorber.

The electromagnetic cascades include the effect of a long-lived isomeric state ($t_{1/2} \approx 100$ ns) of ^{236}U at 1.05 MeV [62] that distorts the ^{235}U(n, γ) spectra measured by the TAC. The effect is clearly visible in Fig. 12, where two peaks separated by 1 MeV appear at high energies instead of a single peak around the neutron separation energy [$S_n(n + ^{235} U) = 6.5$ MeV]. The population of the isomer was estimated to be 15% of the total neutron capture reactions, when fitting the LANSCE experimental data [7].

F. Pile-up corrections

There is no pile-up in the FTMG detectors, since there the counting rates are low compared to the width of the signals. On the contrary, the dead material interposed in the beam due to the FTMG detectors produced a counting rate in the TAC high enough to induce pile-up effects. These pile-up effects can be identified easily by performing the ratio between the number of counts in coincidence between both detection systems and the total number of counts in the FTMG detectors, $c_{tag}(E_n)/c_{tot,f}(E_n)$, as a function of neutron energy. In absence of pile-up effects, this ratio should be constant (note that $c_{bkg,f} = 0$). However, this is not what we observe in our measurement, as shown in Fig. 13.

Due to the high counting rates some of the signals in the TAC are no longer detected and others are detected with a modified energy. As a result, some TAC events are detected with modified E_{sum} and/or m_{cr} values. The pile-up effects increase with neutron energy, as the counting rate does. As shown in Fig. 13, the number of counts in coincidence between both detection systems (c_{tag}) can both decrease [Fig. 13(a)] and increase [Fig. 13(b)] with respect to the number of counts in the FTMG detectors ($c_{tot,f}$), depending on the cuts in E_{sum} and m_{cr}.

The pile-up in the n_TOF TAC has already been studied in previous works [63,64]. For this analysis we used a pile-up correction model very similar to that used in Ref. [45]. This model is based on the same principles as described in Ref. [63], and a more detailed description can be found in Ref. [49]. Figure 13 shows how the model can reproduce some of the experimentally observed effects of the pile-up. In Fig. 14 we then show the size of the pile-up corrections, obtained with the model, for three different cuts in the energy range of our measurement, including the cuts used for this analysis ($2 < m_{cr} < 6$). The uncertainty in this correction has been estimated to be 10% by comparing predictions of the model with several experimentally observed pile-up effects, such as those of Fig. 13.

G. Normalization

The α-ratio measurement is an absolute measurement and does not require any type of normalization.

The energy dependence of the capture cross section, obtained from Eq. (4), has been normalized to the well-known integral of the ^{235}U(n, f) cross section from 7.8 to 11 eV of 247.5(30) b eV [65]. We have used the thin target approximation, $Y_x(E_n) \simeq n_s \sigma_x(E_n)$, as mentioned at the beginning of Sec. IV. The ratio between the capture and fission cross

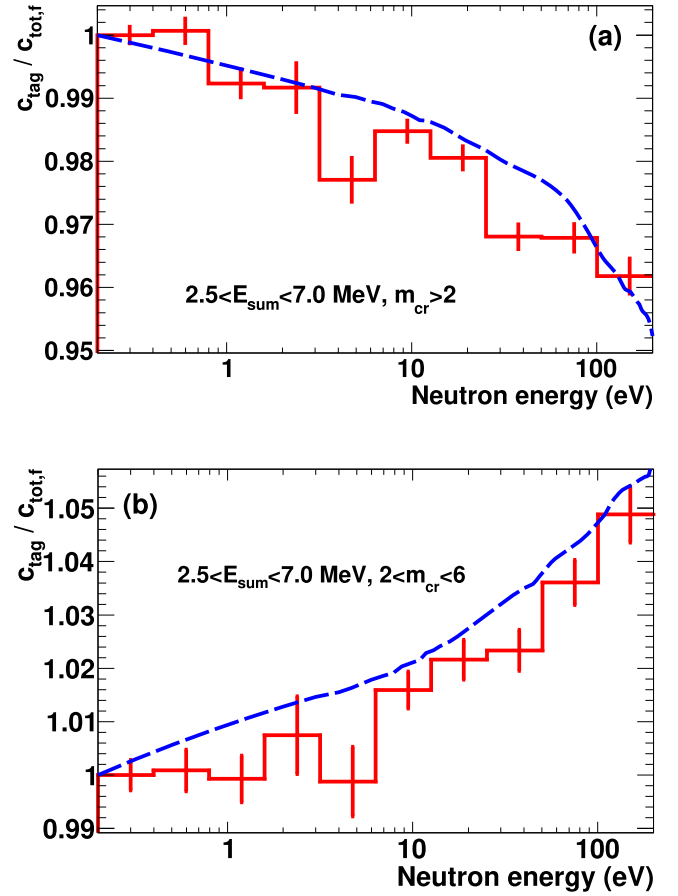

FIG. 13. Ratio between the number of counts in coincidence between both detection systems (c_{tag}) and the number of counts in the FTMG detectors ($c_{tot,f}$), as a function of neutron energy and for two different cuts in the TAC events. The experimental values are shown in histograms, whose error bars are due to the counting statistics. They have been normalized to the content of the first bin. The dotted lines correspond to the predictions of the pile-up model developed for this work.

sections integrated between energies E_1 and E_2 is then

$$\frac{\int_{E_1}^{E_2} \sigma_\gamma dE_n}{\int_{E_1}^{E_2} \sigma_f dE_n} = \frac{\varepsilon_f}{\varepsilon_\gamma} \frac{\int_{E_1}^{E_2} \frac{c_{aco,\gamma} - \frac{1-\varepsilon_f}{\varepsilon_f} c_{tag} - c_{\alpha th,\gamma}}{\phi_N} dE_n}{\int_{E_1}^{E_2} \frac{c_{aco,f} + c_{tag}}{\phi_N} dE_n}, \quad (10)$$

where we assumed that $\varepsilon_f^* = \varepsilon_f$ (see Sec. IV D), and that ε_γ and ε_f do not depend on neutron energy. The dependence on neutron energy of the rest of the variables is not shown explicitly.

We have normalized the capture data according to Eq. (10), and the achieved uncertainty in the normalization process, mainly due to counting statistics, is 0.4%. The uncertainty in the integral of the ^{235}U(n, f) cross section from 7.8 to 11 eV provided by Ref. [65] is 1.2%. Therefore, the quadratic sum of both values leads to an uncertainty in the normalization of the capture cross section of 1.3%.
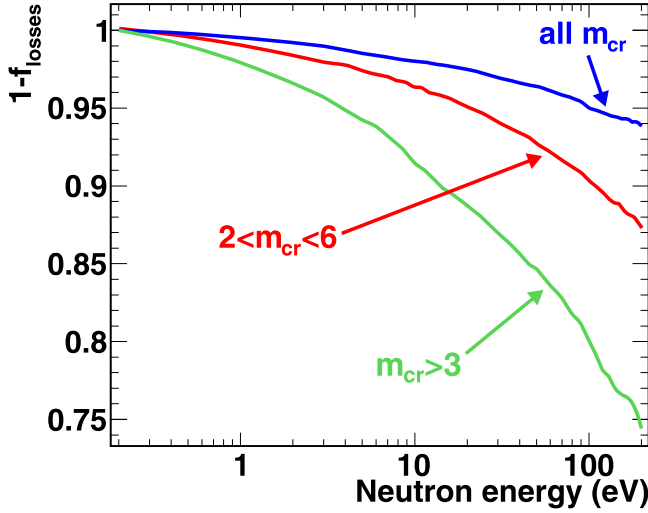
FIG. 14. One minus the fraction of ^{235}U(n, γ) events lost (f_{losses}) due to the pile-up, as a function of neutron energy. Three different cuts have been considered, all of them with $2.5 < E_{sum} < 7$ MeV but with different m_{cr} conditions.

V. RESULTS

A. Uncertainties

We considered the following uncertainties due to systematic effects in the calculation of the α ratio and the capture cross section:

(i) Uncertainty in ε_f (equal to ε_f^*), which is $\Delta\varepsilon_f = 1.2\%$ (Sec. IV D).

(ii) Uncertainty in ε_γ, which is $\Delta\varepsilon_\gamma = 1.7\%$ (Sec. IV E).

(iii) Uncertainty in the normalization to the ^{235}U fission cross section from 7.8 to 11 eV (Δnorm), which is 1.3% (Sec. IV G).

(iv) Uncertainty in the background related with the interaction of the neutron beam with materials different than the ^{235}U targets (Δbkg). This background was obtained from dedicated measurements, but we had to perform some corrections (Sec. IV B). This contribution corresponds to the propagation of the uncertainty in these corrections to the α ratio and the capture cross section.

(v) Uncertainty due to the pile-up corrections (Δpile-up), which is 10% of the correction (Sec. IV F).

Other sources of uncertainties, such as the calculation of the background related with the delayed detection of the fission reactions (Fig. 6) or the neutron fluence shape, were considered small enough to be neglected.

The propagation of these uncertainties to the measured capture cross section is presented in Fig. 15, where the cross section is integrated in ten isolethargic intervals between 0.2 and 200 eV. The uncertainties due to ε_γ and the normalization were added quadratically. The uncertainty due to counting statistics is also shown, with the same binning and labeled as Δstat.

The propagation of these uncertainties to the measured α ratio is the same as for the capture cross section for the $\Delta\varepsilon_\gamma$,
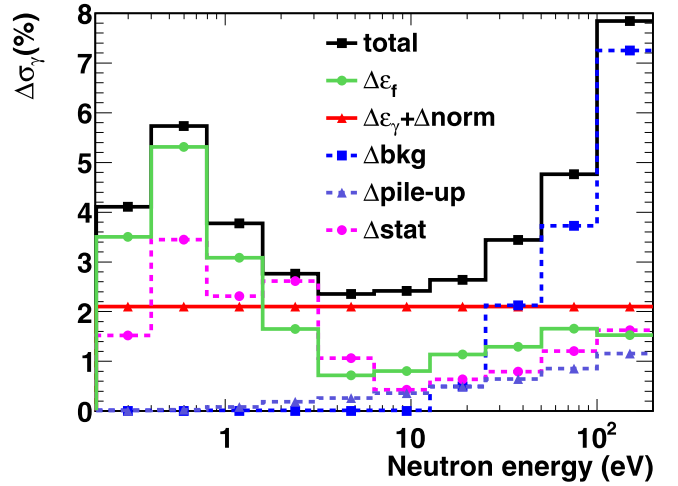

FIG. 15. Magnitude of the different sources of uncertainty in the capture cross section, as a function of neutron energy. The total uncertainty was calculated as the quadratic sum of the ε_f, ε_γ, Δbkg, Δnorm, and Δpile-up contributions; it corresponds to the total uncertainty due to systematic effects.

Δbkg, and Δpile-up contributions. In the case of $\Delta\varepsilon_f$, an extra 1.2% ($\Delta\varepsilon_f = 1.2\%$) has to be added to the one obtained from the capture cross section. This extra contribution can be easily deduced from Eqs. (4) and (5). The normalization uncertainty (Δnorm) is not relevant for the α ratio.

The major contribution to the final uncertainty comes from the background subtraction, both due to the fission reactions and to the background related with the interaction of the neutron beam with materials different than the ^{235}U targets. In both these sources there is an effect in the counting statistics as well as in the uncertainties due to systematic effects. The impact of both contributions on the measured capture cross section and α ratio depends on neutron energy. In the case of the background due to fission this dependence is related to the variation of the capture-to-fission cross-section ratio. A narrower binning on Fig. 15 leads to larger fluctuations in this contribution. The contribution of the background related with the interaction of the neutron beam with materials different than the ^{235}U targets is larger as the neutron energy increases. In fact, it is the one that limits the measurement to 200 eV. It should also be borne in mind that in a resonance analysis this contribution will be somewhat smaller than that shown in Fig. 15, since the valleys between resonances will have less impact.

B. Comparison with evaluated libraries and previous measurements

The most recent nuclear data libraries adopt values from three different evaluations of the capture and fission cross sections in the energy range of this measurement. Two libraries (ENDF/B-VIII.0 and JEFF-3.3) adopted two different versions of the CIELO files [11]; the third evaluation, described in detail in Ref. [66], is the one adopted by most of the rest of the libraries: ENDF/B-VII.1 [67], JEFF-3.2 [68], JENDL-4.0 [69], BROND-3.1 [70], and CENDL-3.1 [71].
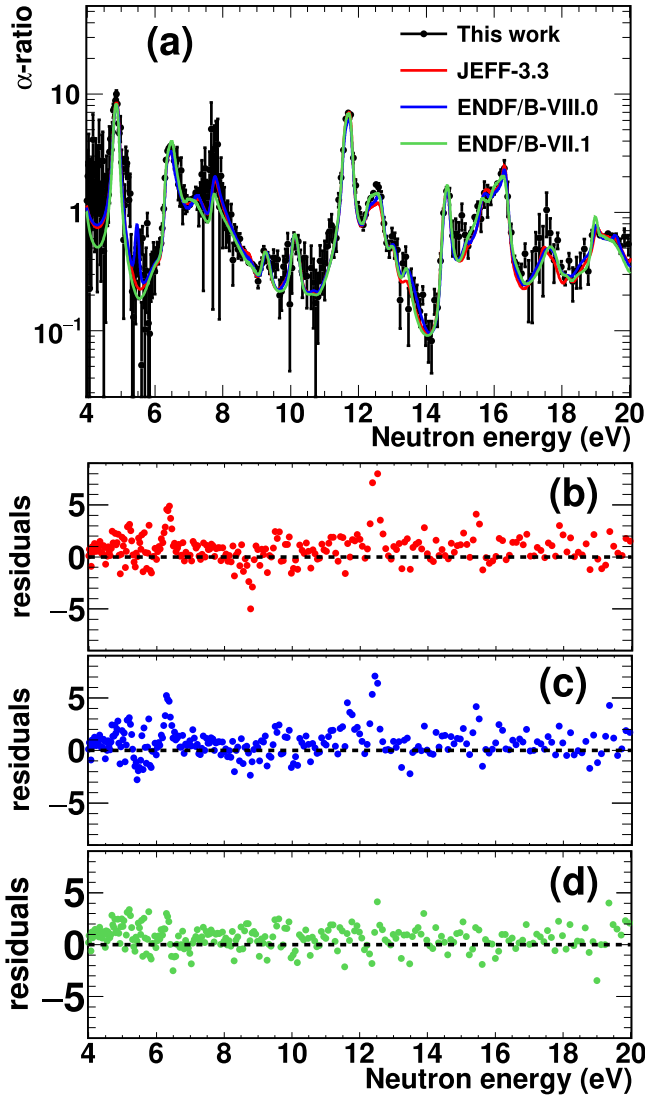
FIG. 16. (a) α ratio of ^{235}U obtained in this work together with those in the JEFF-3.3, ENDF/B-VIII.0, and ENDF/B-VII.1 data libraries, between 4 and 20 eV. The error bars correspond to uncertainties due to counting statistics. The residuals (measured minus evaluated divided by the uncertainty due to counting statistics) in comparison with (b) JEFF-3.3, (c) ENDF/B-VIII.0, and (d) ENDF/B-VII.1 are also shown.

A comparison of the α ratio obtained in this work and the three aforementioned evaluations is provided in Fig. 16. In the energy range shown, between 4 and 20 eV, the largest differences between the data obtained in this work and the evaluations are in the resonances at 6.3 and 12.4 eV. The differences are larger with respect to JEFF-3.3 and ENDF/B-VIII.0 than to ENDF/B-VII.1. In addition, what is more important, the residuals clearly show that the α ratio obtained in this work is, on average, larger than the evaluated ones.

The cross sections obtained in this work have been integrated in ten isolethargic intervals between 0.2 and 200 eV, the same as in Fig. 15, and compared with the evaluations in Fig. 17. Four different comparisons are presented. One of them [Fig. 17(a)] is the capture cross section, and the other

three are ratios between evaluated data and the results obtained in this work. These ratios are between the capture cross sections [Fig. 17(b)], the fission cross sections [Fig. 17(c)], and the ratio between them [Fig. 17(d)].

The comparison shows that the capture cross section obtained in this work has a similar shape to ENDF/B-VII.1 above 0.5 eV, but is around 10% larger. It is in general compatible with the evaluations used by ENDF/B-VIII.0 and JEFF-3.3 below 4 eV and above 100 eV. Between 4 and 100 eV, it is around 10% larger, as in the case of ENDF/B-VII.1.

The fission cross section is compatible with JEFF-3.3 and ENDF/B-VIII.0 within 2% and 3%, respectively. However, it is up to 6% larger than ENDF/B-VII.1. The differences between evaluations are up to 4% for fission.

The comparison between the capture-to-fission cross-section ratios shows a similar trend to the comparison between the capture cross sections. However, in this case the differences between the evaluations and the values obtained in this work are smaller in the energy range between 4 and 100 eV.

To see if the same discrepancy between 4 and 100 eV is observed in other experiments, we also compared the results obtained in this work with previous ^{235}U(n, γ) cross-section measurements [7,8,18,72,73]. Unlike this measurement, all of them normalize their results to a previously existing measured or evaluated capture cross section. The data from Danon *et al.* [8] have been normalized to the thermal point (0.0253 eV) and the resonances at 11.7 and 19 eV. They obtained a capture cross section between 10 and 150 eV which is, on average, 4% smaller than ENDF/B-VII.1. The data from Jandel *et al.* [7], Gwin *et al.* [73], Perez *et al.* [72], and De Saussure *et al.* [18] were normalized, respectively, to previously measured or evaluated capture cross sections in the 45–100, 0.02–0.4, 100–200, and 0.4–1 eV energy ranges. The ratio between these results and the capture cross section obtained in this work is presented in Fig. 18. The cross section from Gwin *et al.* [73] is in good agreement with the results of this work, whereas the other three measurements are closer to the evaluated cross sections. It is worth mentioning, however, that the authors of Ref. [73] recommended in a later article [74] not to use the data from Ref. [73]. They argued that the ^{235}U fission cross section reported in Ref. [73], together with the capture cross section, is not in agreement with other ^{235}U(n, f) measurements they performed afterwards. In particular, the fission cross section reported in Ref. [74] is 4% larger in the 0.02–10 eV energy region than the one in Ref. [73].

A more detailed comparison with the evaluations is presented in Figs. 19 and 20, where we compare the pointwise capture cross section obtained in this work with that in JEFF-3.3. In addition, we show the ratios between the cross-section resonance integrals in the JEFF-3.3, ENDF/B-VIII.0, and ENDF/B-VII.1 data libraries and the ones obtained in this work. The ratio values are shown as points (circles, squares, and triangles), uncertainties due to counting statistics as vertical error bars, and uncertainties due to $\Delta\varepsilon_f$ and Δnorm as horizontal error bars. The integration energy interval is given by these horizontal bars.
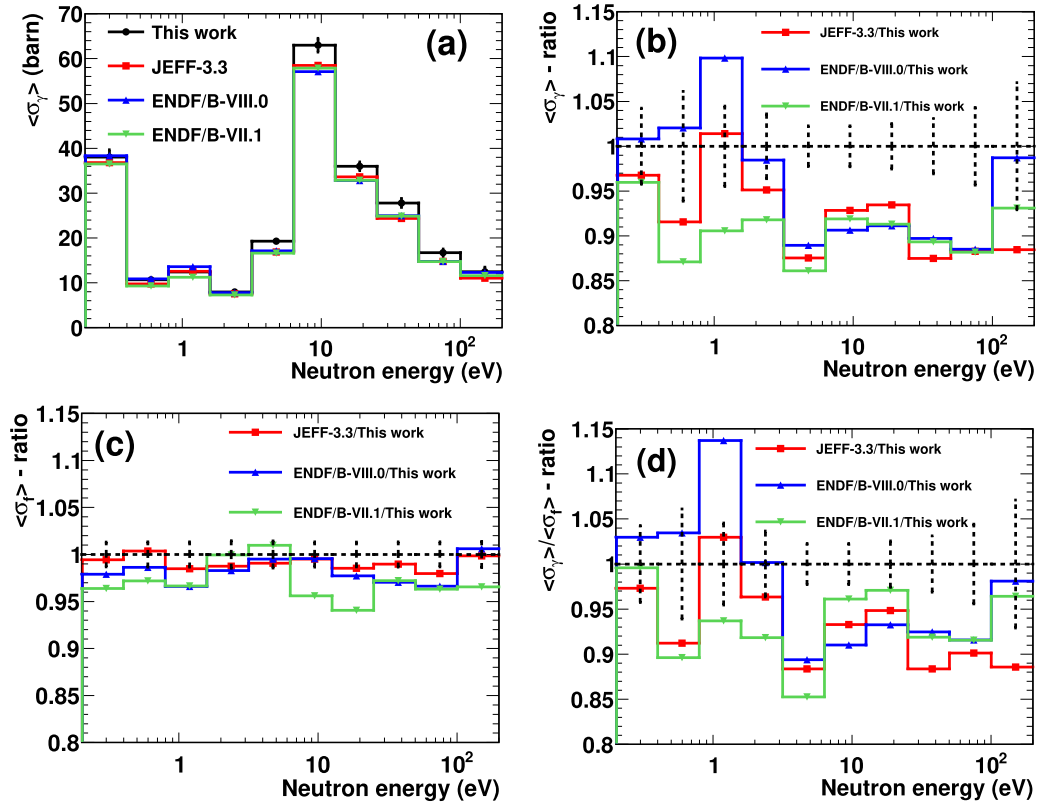
FIG. 17. Average ^{235}U capture ($x = \gamma$) and fission ($x = f$) cross sections $\langle \sigma_x \rangle = \int_{E_1}^{E_2} \sigma_x(E) dE / (E_2 - E_1)$ obtained in this work together with those in the JEFF-3.3, ENDF/B-VIII.0, and ENDF/B-VII.1 data libraries. In particular, the figures show (a) the capture cross section and the ratios between the evaluated values and those obtained in this work for (b) the capture cross section, (c) the fission cross section, and (d) the ratio between them. The uncertainties shown correspond to the quadratic sum of those from counting statistics and systematic effects (Fig. 15). In (b)–(d) the uncertainties are indicated in $y = 1$, and are the same for the three plotted ratios.

VI. SUMMARY AND CONCLUSIONS

We measured the neutron capture-to-fission cross-section ratio (α ratio) and the capture cross section of ^{235}U at the
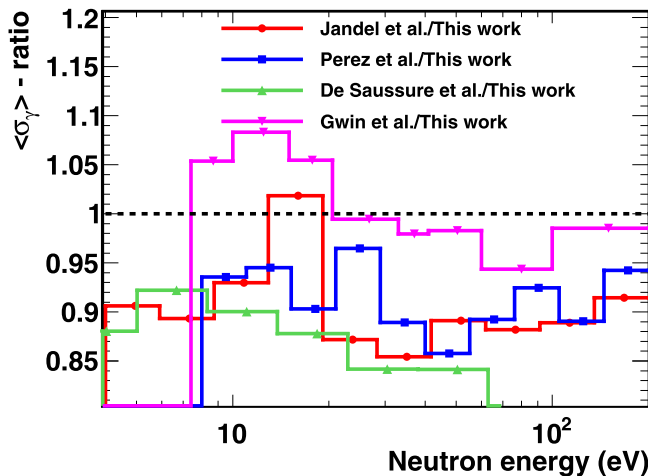

FIG. 18. Ratio between the capture cross sections reported by other ^{235}U(n, γ) cross-section measurements—Jandel *et al.* [7], Perez *et al.* [72], De Saussure *et al.* [18], and Gwin *et al.* [73]—and this work.

CERN n_TOF facility between 0.2 and 200 eV, using the time-of-flight technique. The measurement of the neutron capture cross section of fissile actinides is a challenging task due to the dominant time-correlated γ-ray background produced in the competing fission process. Neutron capture on ^{235}U is a critical reaction channel for nuclear applications.

The measurement was performed with the n_TOF Total Absorption Calorimeter (TAC) in coincidence with micromegas detectors used as fission tagging detectors. We used ten samples that contained 41.15(5) mg of ^{235}U in total. The results of this experiment, along with two other recent capture measurements carried out in LANL [7] and RPI [8], have already been incorporated into a new evaluation of ^{235}U performed within the scope of the CIELO Project.

The α ratio was measured without using any other reference cross section. The capture cross section, obtained with lower statistical fluctuations than the α ratio, has been measured in reference to the shape of the standard ^{6}Li(n, t) cross section and normalized to the integral of the ^{235}U(n, f) cross section between 7.8 and 11 eV. Total uncertainties due to systematic effects in both the α ratio and the capture cross section are, in general, less than 5% below 100 eV. The obtained results are compatible within uncertainties with the most recent evaluations available in ENDF/B-VIII.0 and JEFF-3.3 below 4 eV and above 100 eV. On the contrary, between 4 and
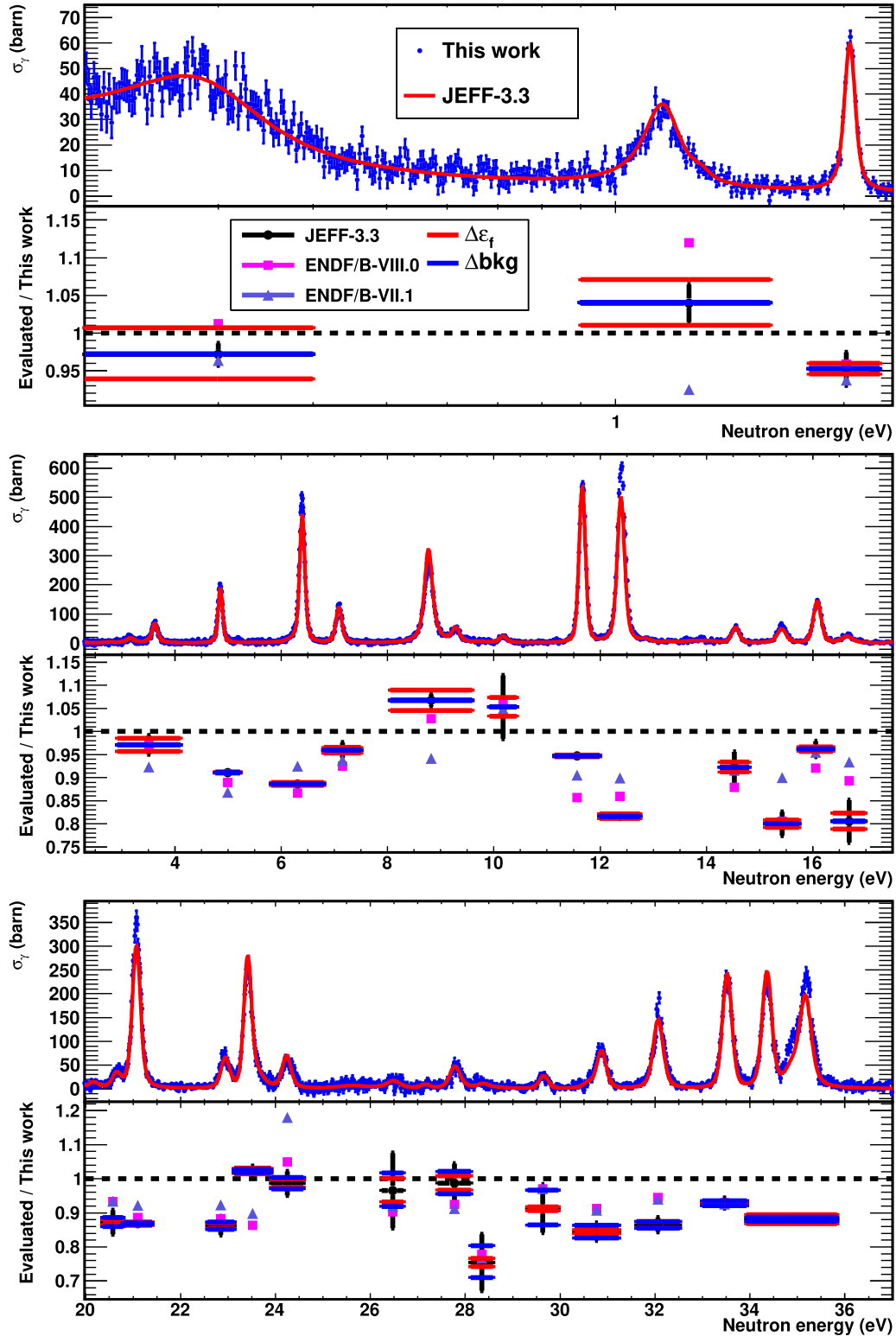
FIG. 19. In the upper panels, capture cross section obtained in this work compared with JEFF-3.3. In the bottom panels, ratio of the evaluated cross-section resonance integrals compared to the experimental data. Uncertainties due to counting statistics are given by the vertical error bars. Uncertainties due to systematic effects associated to the calculation of ε_f and to the subtraction of the background related with the interaction of the neutron beam with materials different than the ^{235}U targets (Δbkg) are given by horizontal error bars, which also define the integration ranges. The uncertainties appear only in the ratios with JEFF-3.3, but they are the same in the ratios with ENDF/B-VIII.0 and ENDF/B-VII.1.
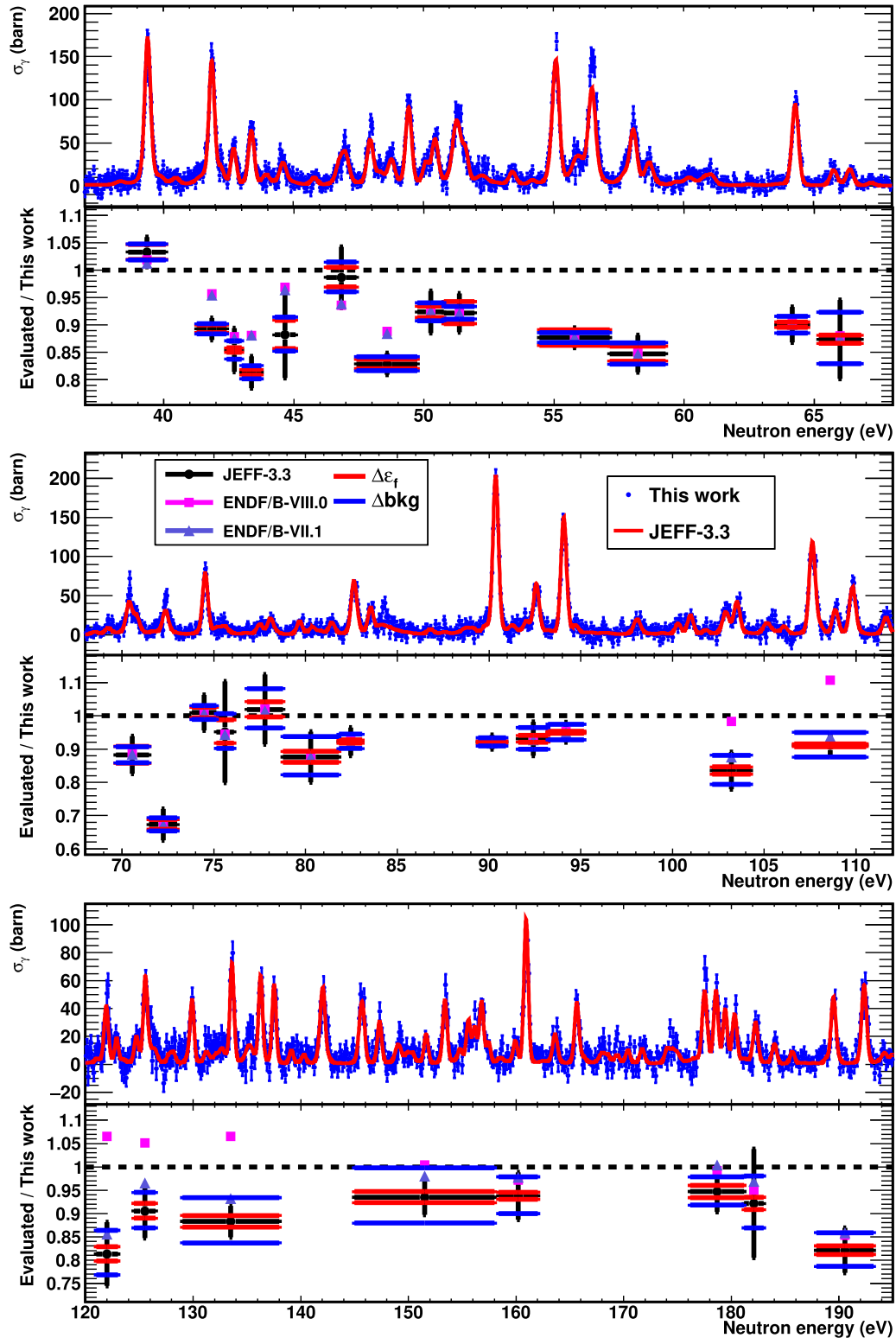
FIG. 20. The same as in Fig. 19 but for different neutron energy range.

100 eV the obtained capture cross section is, on average, 10% larger.

Regarding the measurement technique, we showed that it is in general not correct to assume that the deposited energy spectrum in the γ-ray detector due to fission reactions has the same shape as the spectrum tagged with the charged-particle detector. We observed this effect experimentally in our setup and developed a methodology to correct it. If present, not correcting this effect can produce a large bias in the measurement results.

[1] M. Salvatores *et al.*, NEA/WPEC-26 Technical Report No. 6410 (OECD, Paris, 2008).

[2] G. Aliberti, G. Palmiotti, M. Salvatores, and C. G. Stenberg, Nucl. Sci. Eng. **146**, 13 (2004).

[3] G. Aliberti, G. Palmiotti, M. Salvatores, T. K. Kim, T. A. Taiwo, M. Anitescu, I. Kodeli, E. Sartori, J. C. Bosq, and J. Tommasi, Ann. Nucl. Energy **33**, 700 (2006).

[4] O. Iwamoto *et al.*, NEA/WPEC-29 Technical Report (OECD, Paris, 2011).

[5] A. J. Plompen, T. Kawano, and R. Capote Noy, Technical Report Series INDC(NDS)-0597 (IAEA, Vienna, 2012).

[6] T. Bredeweg, M. Fowler, J. Becker, E. Bond, M. Chadwick, R. Clement, E.-I. Esch, T. Ethvignot, T. Granier, M. Jandel, R. Macri, J. O'Donnell, R. Reifarth, R. Rundberg, J. Ullmann, D. Vieira, J. Wilhelmy, J. Wouters, and C. Wu, Nucl. Instrum. Methods B **261**, 986 (2007).

[7] M. Jandel, T. A. Bredeweg, E. M. Bond, M. B. Chadwick, A. Couture, J. M. O'Donnell, M. Fowler, R. C. Haight, T. Kawano, R. Reifarth, R. S. Rundberg, J. L. Ullmann, D. J. Vieira, J. M. Wouters, J. B. Wilhelmy, C. Y. Wu, and J. A. Becker, Phys. Rev. Lett. **109**, 202506 (2012).

[8] Y. Danon, D. Williams, R. Bahran, E. Blain, B. McDermott, D. Barry, G. Leinweber, R. Block, and M. Rapp, Nucl. Sci. Eng. **187**, 291 (2017).

[9] OECD, Nuclear Energy Agency, Collaborative International Evaluated Library Organisation (CIELO) pilot project, WPEC Subgroup 40 (SG40), https://www.oecd-nea.org/science/wpec/sg40-cielo/.

[10] M. Chadwick *et al.*, Nucl. Data Sheets **118**, 1 (2014).

[11] M. Chadwick *et al.*, Nucl. Data Sheets **148**, 189 (2018).

[12] R. Capote and A. Trkov (coordinators), IAEA CIELO Data Development Project within the International Pilot Project of the OECD/NEA, https://www-nds.iaea.org/CIELO/.

[13] R. Capote *et al.*, Nucl. Data Sheets **148**, 254 (2018).

[14] M. B. Chadwick *et al.*, NEA/WPEC-40 Technical Report No. 7498 (OECD, Paris, 2019).

[15] D. Brown *et al.*, Nucl. Data Sheets **148**, 1 (2018).

[16] G. V. Muradyan, Y. V. Adamchuk, Y. G. Shchepkin, and M. A. Voskanyan, Nucl. Sci. Eng. **90**, 60 (1985).

[17] Y. V. Adamchuk, M. A. Voskanyan, G. Georgiev, A. L. Kovtun, G. V. Muradyan, N. Stancheva, N. Chikov, N. Yaneva, and Y. G. Shchepkin, At. Energy **65**, 1022 (1988).

[18] G. de Saussure *et al.*, *Nuclear Data for Reactors: Proceedings of a Conference on Nuclear Data, Microscopic Cross Sections, and Other Data Basic for Reactors* (IAEA, Vienna, 1967), p. 233.

[19] C. Guerrero *et al.* (n_TOF Collaboration), Eur. Phys. J. A **48**, 29 (2012).

[20] S. Mosby, T. A. Bredeweg, A. Chyzh, A. Couture, R. Henderson, M. Jandel, E. Kwan, J. M. O'Donnell, J. Ullmann, and C. Y. Wu, Phys. Rev. C **89**, 034610 (2014).

[21] S. Mosby, T. A. Bredeweg, A. Couture, M. Jandel, T. Kawano, J. L. Ullmann, R. A. Henderson, and C. Y. Wu, Phys. Rev. C **97**, 041601(R) (2018).

[22] S. Mosby, T. Bredeweg, A. Couture, M. Jandel, T. Kawano, J. Ullmann, R. Henderson, and C. Wu, Nucl. Data Sheets **148**, 312 (2018).

[23] M. Q. Buckner, C. Y. Wu, R. A. Henderson, B. Bucher, N. Wimer, A. Chyzh, T. A. Bredeweg, B. Baramsai, A. Couture, M. Jandel, S. Mosby, and J. L. Ullmann (DANCE Collaboration), Phys. Rev. C **95**, 024610 (2017).

[24] M. Q. Buckner, C. Y. Wu, R. A. Henderson, B. Bucher, N. Wimer, A. Chyzh, T. A. Bredeweg, B. Baramsai, A. Couture, M. Jandel, S. Mosby, and J. L. Ullmann, Phys. Rev. C **95**, 061602(R) (2017).

[25] J. Balibrea-Correa *et al.* (n_TOF Collaboration), EPJ Web Conf. **146**, 11021 (2017).

[26] M. Bacak *et al.*, EPJ Web Conf. **211**, 03007 (2019).

[27] C. Guerrero *et al.* (n_TOF Collaboration), Nucl. Instrum. Methods A **608**, 424 (2009).

[28] S. Andriamonje, M. Calviani, Y. Kadi, R. Losito, V. Vlachoudis, E. Berthoumieux, F. Gunsing, A. Giganon, Y. Giomataris, C. Guerrero, R. Sarmento, P. Schillebeeckx, and P. Siegler, J. Korean Phys. Soc. **59**, 1597 (2011).

[29] C. Guerrero *et al.* (n_TOF Collaboration), Eur. Phys. J. A **49**, 27 (2013).

[30] U. Abbondanno *et al.* (n_TOF Collaboration), CERN Technical Report No. INTC-2002-037 (CERN, 2003).

[31] E. Berthoumieux *et al.* (n_TOF Collaboration), CERN Technical Report No. CERN-n_TOF-PUB-2013-001 (CERN, 2013).

[32] M. Barbagallo *et al.* (n_TOF Collaboration), Eur. Phys. J. A **49**, 156 (2013).

[33] F. Gunsing *et al.* (n_TOF Collaboration), Eur. Phys. J. Plus **131**, 371 (2016).

[34] S. Marrone *et al.* (n_TOF Collaboration), Nucl. Instrum. Methods A **517**, 389 (2004).

[35] Y. Giomataris, P. Rebourgeard, J. Robert, and G. Charpak, Nucl. Instrum. Methods A **376**, 29 (1996).

[36] S. Andriamonje, D. Attie, E. Berthoumieux, M. Calviani, P. Colas, T. Dafni, G. Fanourakis, E. Ferrer-Ribas, J. Galan, T. Geralis, A. Giganon, I. Giomataris, A. Gris, C. G. Sanchez, F. Gunsing, F. J. Iguaz, I. Irastorza, R. D. Oliveira, T. Papaevangelou, J. Ruz, I. Savvidis, A. Teixera, and A. Tomás, J. Instrum. **5**, P02001 (2010).

[37] U. Abbondanno *et al.* (n_TOF Collaboration), Nucl. Instrum. Methods A **538**, 692 (2005).

[38] S. Marrone *et al.*, Nucl. Instrum. Methods A **568**, 904 (2006).

[39] P. Žugec, C. Weiss, C. Guerrero, F. Gunsing, V. Vlachoudis, M. Sabate-Gilarte, A. Stamatopoulos, T. Wright, J. Lerendegui-Marco, F. Mingrone, J. Ryan, S. Warren, A. Tsinganis, and M. Barbagallo, Nucl. Instrum. Methods A **812**, 134 (2016).

[40] J. Heyse, M. Anastasiou, R. Eykens, A. Moens, A. Plompen, P. Schillebeeckx, G. Sibbens, D. Vanleeuw, and R. Wynants, Nucl. Data Sheets **119**, 407 (2014).

[41] C. Massimi *et al.* (n_TOF Collaboration), Phys. Rev. C **81**, 044616 (2010).

[42] C. Guerrero *et al.* (n_TOF Collaboration), Phys. Rev. C **85**, 044616 (2012).

[43] E. Mendoza *et al.* (n_TOF Collaboration), Phys. Rev. C **90**, 034608 (2014).

[44] T. Wright *et al.* (n_TOF Collaboration), Phys. Rev. C **96**, 064601 (2017).

[45] E. Mendoza *et al.* (n_TOF Collaboration), Phys. Rev. C **97**, 054616 (2018).

[46] OECD/NEA Data Bank, JEFF-3.3 (2017), https://www.oecd-nea.org/dbdata/jeff/jeff33/index.html.

[47] A. J. M. Plompen *et al.*, Eur. Phys. J. A **56**, 181 (2020).

[48] S. Amaducci *et al.* (n_TOF Collaboration), Eur. Phys. J. A **55**, 120 (2019).

[49] J. Balibrea, Ph.D. thesis, Universidad Complutense de Madrid, 2017.

[50] V. Stavinsky and M. Shaker, Nucl. Phys. **62**, 667 (1965).

[51] J. Lynn, Phys. Lett. **18**, 31 (1965).

[52] P. Talou, J. E. Lynn, T. Kawano, S. Mosby, A. Couture, and O. Bouland, EPJ Web Conf. **122**, 01013 (2016).

[53] E. Browne and J. Tuli, Nucl. Data Sheets **107**, 2649 (2006).

[54] A. Elwyn and A. Ferguson, Nucl. Phys. A **148**, 337 (1970).

[55] K.-H. Schmidt, B. Jurado, C. Amouroux, and C. Schmitt, Nucl. Data Sheets **131**, 107 (2016).

[56] M. M. Hoffman, Phys. Rev. **133**, B714 (1964).

[57] S. Zeynalov, F.-J. Hambsch, and S. Obertstedt, J. Korean Phys. Soc. **59**, 1396 (2011).

[58] F. Bečvář, Nucl. Instrum. Methods A **417**, 434 (1998).

[59] S. Agostinelli *et al.* (GEANT4 Collaboration), Nucl. Instrum. Methods A **506**, 250 (2003).

[60] J. Allison *et al.*, Nucl. Instrum. Methods A **835**, 186 (2016).

[61] C. Guerrero, D. Cano-Ott, E. Mendoza, J. Taín, A. Algora, E. Berthoumieux, N. Colonna, C. Domingo-Pardo, E. González-Romero, M. Heil, D. Jordán, F. Käppeler, C. Lampoudis, T. Martínez, C. Massimi, and R. Plag, Nucl. Instrum. Methods A **671**, 108 (2012).

[62] V. Andersen, C. Christensen, and J. Borggreen, Nucl. Phys. A **269**, 338 (1976).

[63] E. Mendoza, D. Cano-Ott, C. Guerrero, and E. Berthoumieux, Nucl. Instrum. Methods A **768**, 55 (2014).

[64] C. Guerrero, D. Cano-Ott, E. Mendoza, and T. Wright, Nucl. Instrum. Methods A **777**, 63 (2015).

[65] A. Carlson, V. Pronyaev, R. Capote, G. Hale, Z.-P. Chen, I. Duran, F.-J. Hambsch, S. Kunieda, W. Mannhart, B. Marcinkevicius, R. Nelson, D. Neudecker, G. Noguere, M. Paris, S. Simakov, P. Schillebeeckx, D. Smith, X. Tao, A. Trkov, A. Wallner, and W. Wang, Nucl. Data Sheets **148**, 143 (2018).

[66] L. C. Leal, H. Derrien, N. M. Larson, and R. Q. Wright, Nucl. Sci. Eng. **131**, 230 (1999).

[67] M. Chadwick *et al.*, Nucl. Data Sheets **112**, 2887 (2011).

[68] OECD/NEA Data Bank, JEFF-3.2 (2014), http://www.oecd-nea.org/dbforms/data/eva/evatapes/jeff_32/.

[69] K. Shibata, O. Iwamoto, T. Nakagawa, N. Iwamoto, A. Ichihara, S. Kunieda, S. Chiba, K. Furutaka, N. Otuka, T. Ohsawa, T. Murata, H. Matsunobu, A. Zukeran, S. Kamada, and J. Katakura, J. Nucl. Sci. Technol. **48**, 1 (2011).

[70] A. Blokhin, E. Gai, A. Ignatyuk, I. Koba, V. Manokhin, and V. Pronyaev, Vopr. Atom. Nauki Tekh. Ser. Yad. Konstanty **2**, 62 (2016).

[71] Z. Ge, Z. Zhao, H. Xia, Y. Zhuang, T. Liu, J. Zhang, and H. Wu, J. Korean Phys. Soc. **59**, 1052 (2011).

[72] R. B. Perez, G. de Saussure, E. G. Silver, R. W. Ingle, and H. Weaver, Nucl. Sci. Eng. **52**, 46 (1973).

[73] R. Gwin, E. G. Silver, R. W. Ingle, and H. Weaver, Nucl. Sci. Eng. **59**, 79 (1976).

[74] R. Gwin, R. R. Spencer, R. W. Ingle, J. H. Todd, and S. W. Scoles, Nucl. Sci. Eng. **88**, 37 (1984).